NASA/TM—2014-218321

Radioisotope Stirling Engine Powered Airship for Atmospheric and Surface Exploration of Titan

Anthony J. Colozza
Vantage Partners, LLC, Brook Park, Ohio

Robert L. Cataldo
Glenn Research Center, Cleveland, Ohio

July 2014

NASA STI Program . . . in Profile

Since its founding, NASA has been dedicated to the advancement of aeronautics and space science. The NASA Scientific and Technical Information (STI) program plays a key part in helping NASA maintain this important role.

The NASA STI Program operates under the auspices of the Agency Chief Information Officer. It collects, organizes, provides for archiving, and disseminates NASA's STI. The NASA STI program provides access to the NASA Aeronautics and Space Database and its public interface, the NASA Technical Reports Server, thus providing one of the largest collections of aeronautical and space science STI in the world. Results are published in both non-NASA channels and by NASA in the NASA STI Report Series, which includes the following report types:

- TECHNICAL PUBLICATION. Reports of completed research or a major significant phase of research that present the results of NASA programs and include extensive data or theoretical analysis. Includes compilations of significant scientific and technical data and information deemed to be of continuing reference value. NASA counterpart of peer-reviewed formal professional papers but has less stringent limitations on manuscript length and extent of graphic presentations.

- TECHNICAL MEMORANDUM. Scientific and technical findings that are preliminary or of specialized interest, e.g., quick release reports, working papers, and bibliographies that contain minimal annotation. Does not contain extensive analysis.

- CONTRACTOR REPORT. Scientific and technical findings by NASA-sponsored contractors and grantees.

- CONFERENCE PUBLICATION. Collected papers from scientific and technical conferences, symposia, seminars, or other meetings sponsored or cosponsored by NASA.

- SPECIAL PUBLICATION. Scientific, technical, or historical information from NASA programs, projects, and missions, often concerned with subjects having substantial public interest.

- TECHNICAL TRANSLATION. English-language translations of foreign scientific and technical material pertinent to NASA's mission.

Specialized services also include creating custom thesauri, building customized databases, organizing and publishing research results.

For more information about the NASA STI program, see the following:

- Access the NASA STI program home page at *http://www.sti.nasa.gov*

- E-mail your question to *help@sti.nasa.gov*

- Fax your question to the NASA STI Information Desk at 443–757–5803

- Phone the NASA STI Information Desk at 443–757–5802

- Write to:
  STI Information Desk
  NASA Center for AeroSpace Information
  7115 Standard Drive
  Hanover, MD 21076–1320

NASA/TM—2014-218321

Radioisotope Stirling Engine Powered Airship for Atmospheric and Surface Exploration of Titan

Anthony J. Colozza
Vantage Partners, LLC, Brook Park, Ohio

Robert L. Cataldo
Glenn Research Center, Cleveland, Ohio

National Aeronautics and
Space Administration

Glenn Research Center
Cleveland, Ohio 44135

July 2014

Level of Review: This material has been technically reviewed by technical management.

Available from

NASA Center for Aerospace Information
7115 Standard Drive
Hanover, MD 21076–1320

National Technical Information Service
5301 Shawnee Road
Alexandria, VA 22312

Available electronically at http://www.sti.nasa.gov

Contents

Radioisotope Stirling Engine Powered Airship for Atmospheric and Surface Exploration of Titan

Anthony J. Colozza
Vantage Partners, LLC
Brook Park, Ohio 44142

Robert L. Cataldo
National Aeronautics and Space Administration
Glenn Research Center
Cleveland, Ohio 44135

Abstract

The feasibility of an advanced Stirling radioisotope generator (ASRG) powered airship for the near surface exploration of Titan was evaluated. The analysis did not consider the complete mission only the operation of the airship within the atmosphere of Titan. The baseline airship utilized two ASRG systems with a total of four general-purpose heat source (GPHS) blocks. Hydrogen gas was used to provide lift. The ASRG systems, airship electronics and controls and the science payload were contained in a payload enclosure. This enclosure was separated into two sections, one for the ASRG systems and the other for the electronics and payload. Each section operated at atmospheric pressure but at different temperatures. The propulsion system consisted of an electric motor driving a propeller. An analysis was set up to size the airship that could operate near the surface of Titan based on the available power from the ASRGs. The atmospheric conditions on Titan were modeled and used in the analysis. The analysis was an iterative process between sizing the airship to carry a specified payload and the power required to operate the electronics, payload and cooling system as well as provide power to the propulsion system to overcome the drag on the airship. A baseline configuration was determined that could meet the power requirements and operate near the Titan surface. From this baseline design additional trades were made to see how other factors affected the design such as the flight altitude and payload mass and volume.

1.0 Introduction

Titan, shown in Figure 1, is the largest moon of Saturn. It is approximately 50 percent larger than Earth's moon and is the only known moon in the solar system to have a significant atmosphere. Its atmospheric pressure near the surface is approximately 1.45 times that of Earth's and the surface temperature is around 94 K (–180 °C). The atmosphere is comprised mainly of nitrogen and is completely covered with clouds and haze. Wind speeds near the surface based on the Huygens probe are low less than 1 m/s. Other than accommodating the low atmospheric temperature, operation on Titan is ideal for an airship. The dense atmosphere can provide significant lift and the low wind speed near the surface minimizes the required propulsion power for controlled flight. The nitrogen atmosphere is non-corrosive and would be compatible with most materials.

To date the exploration of Titan has consisted mainly of images and data taken from flyby probes such as the Voyager series and the Cassini Saturn orbiter. The Huygens probe was the only vehicle to enter the atmosphere and provide data from beneath the cloud cover, as shown in Figure 1. The data and images from the Huygens probe showed a dynamic surface environment with interesting geologic features not that dissimilar to Earth. The Huygens probe however supplied data only for a few hours and most of this was during the descent phase of its mission.

To perform a more detailed evaluation of Titan a long duration vehicle is needed, one that can move around on or near the surface in a controlled manner and over the unpredictable surface terrain of Titan that includes steep inclines, liquid methane lakes, mountain ranges and rocks. An airship is the ideal platform to accomplish this type of mission.

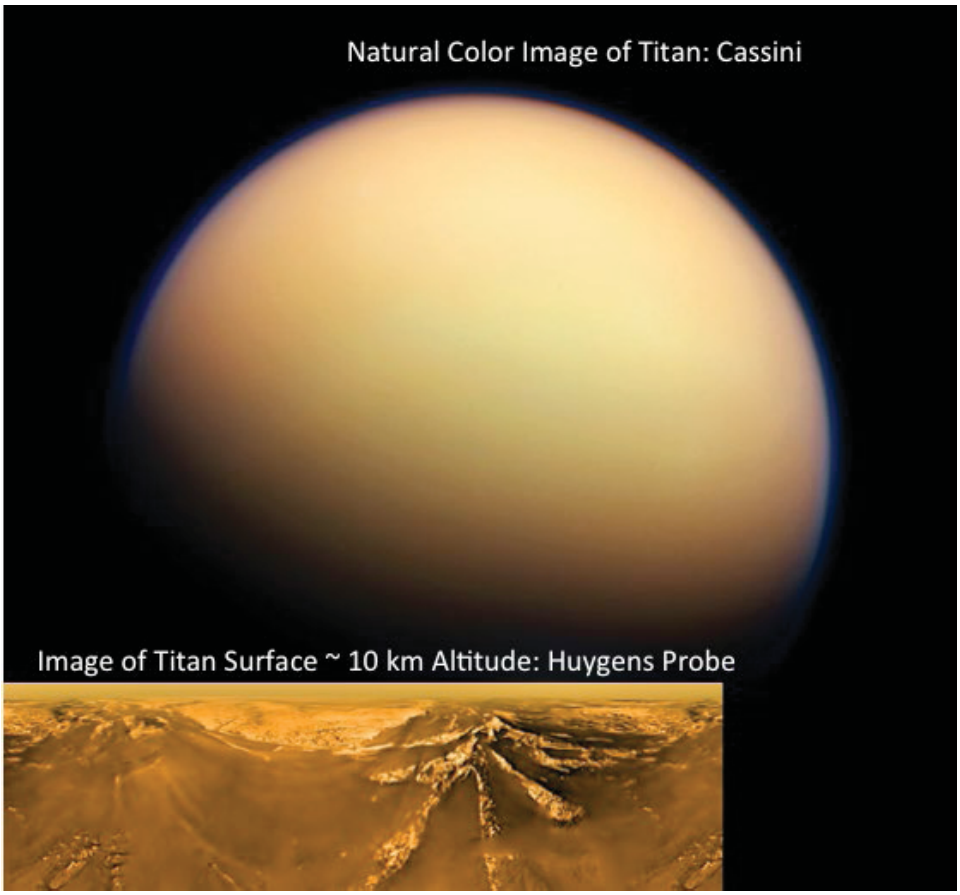

Figure 1.—True color image of Titan from Cassini (Ref. 1) and surface image from the Huygens Probe (Ref. 1).

Wheeled rovers have previously been the only type of mobile vehicles used for planetary exploration and these have only been utilized on the Moon (Russian Lunokhod series, U.S. Apollo Rover) and Mars (Pathfinder: Sojourner, MER: Spirit and Opportunity, MSL: Curiosity) On Mars photovoltaic arrays were utilized as the main power source for all of the rovers except Curiosity which utilized a multi-mission radioisotope thermoelectric generator (MMRTG). However on Titan, due to its distance from the Sun and the thick cloud and haze cover encompassing the moon, utilizing solar power is not feasible. Therefore a different power source is required, one similar to the MMRTG that can convert the heat generated through radioactive decay of Plutonium to electricity. These radioisotope heat sources are commonly utilized for deep space missions, where insufficient solar energy is available, and similarly can be utilized for a Titan surface mission. The one downside to a radioisotope based power system is that they tend to be heavier than that of a typical PV based system. This is critical since for a mobile vehicle the lower its mass, the less power will be required to move. Therefore, maximizing the thermal to electrical conversion efficiency is a critical factor in the power system design. Of the available thermal to electrical conversion systems, a Stirling engine based ASRG provides the highest efficiency and therefore the greatest benefit to the airship.

The thick, dense atmosphere of Titan provides both benefits and obstacles in the design of a surface or near surface vehicle. One advantage is that the high surface density enables the possibility of utilizing a low speed flight vehicle such as an airship, whereas on Mars this option is not feasible (Ref. 2). For Titan an airship provides a number of benefits to scientific exploration. The main advantages include:

- The ability to cover large amounts of surface terrain.
- The capability to descend to the surface and perform scientific investigation at various locations.

- The ability to go over or around obstacles and explore terrain features that would not be accessible to surface vehicles.
- The ability to sample the atmosphere over a range of altitudes.

Although the high surface density is an advantage for an airship in generating lift, the higher pressure and cold temperature may pose problems for operating equipment and electronics. Therefore the electronics and payload must be contained in a heated payload enclosure in order to survive for an extended period of time near the surface. The need for heating adds significantly to the power requirements of the vehicle, increasing its mass and size.

Overall an airship could provide a unique capability for exploring the surface of Titan. Although technically challenging, as the design and development of any surface vehicle would be, the airship platform could provide significant terrain coverage as well as the means to explore and sample both the surface and lower atmosphere. This capability would provide unequaled science data return and therefore should be thoroughly examined as an option for Titan exploration. The analysis and results discussed in this report are a first step in evaluating the feasibility and capabilities of an ASRG powered Titan airship concept.

2.0 Environment on Titan

The environmental conditions on Titan are very unique and unlike those on any other known planet or moon. In ways it is very Earth like. It has a mostly nitrogen atmosphere, clouds, lakes, rivers and rain. However, with a surface temperature of under 100 K the free liquid is not water but methane. The low atmospheric temperature also lowers the speed of sound through the atmosphere. Near the surface the speed of sound is approximately half that on Earth. Due to the distance from the Sun, cloud cover and haze, little sunlight reaches the surface. The atmospheric density at the surface is 5 times that of Earth and the pressure is 1.5 times greater than that at Earth's surface. A diagram of the atmosphere is shown in Figure 2 and select properties of Titan are given in Table 1.

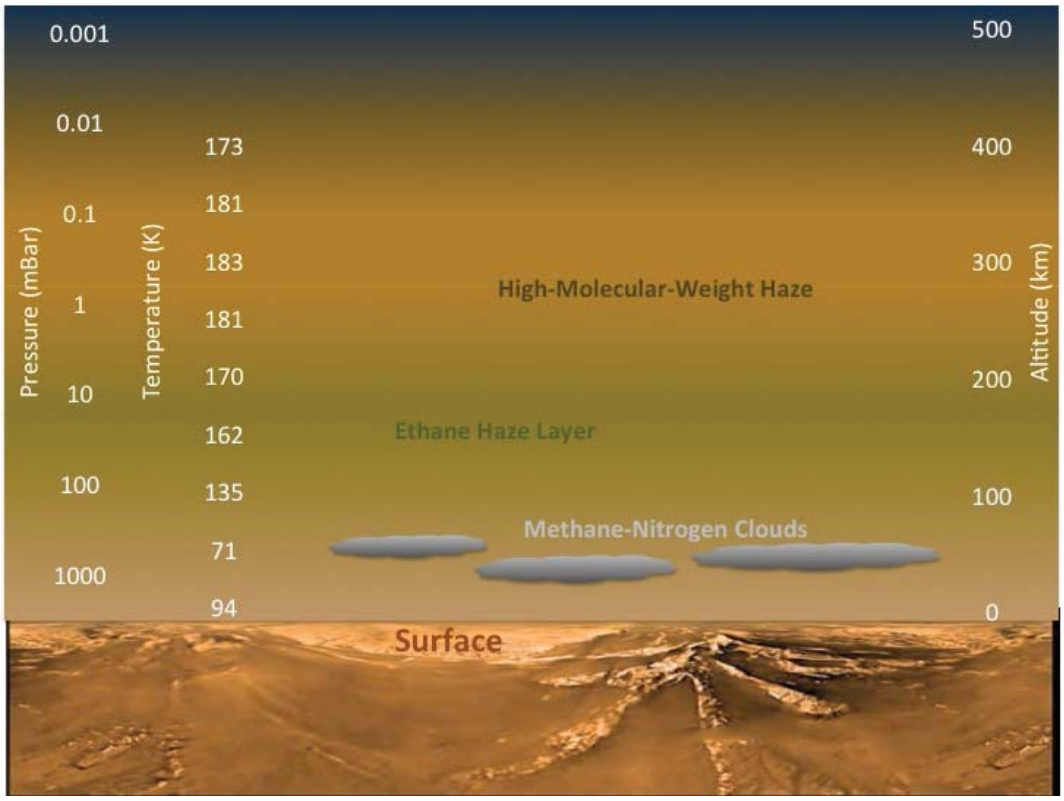

Figure 2.—Illustration of Titan Atmosphere (Refs. 3 and 4).

TABLE 1.—PHYSICAL AND ORBITAL PROPERTIES OF TITAN (REFS. 4, 5, AND 6)

Property	Value
Maximum inclination of equator to orbit to Saturn (δ_{max})	0.35°
Orbital eccentricity (ε)	0.0288
Mean radius of orbit (r_m) around Saturn	1.22×10^6 km
Day period (synchronous to the orbital period around Saturn)	15.95 (Earth days)
Surface pressure	146.7 kPa
Albedo	0.22
Gravitational constant (g_v)	1.35 m/s^2
Orbital period around Saturn	15.95 (Earth days)
Surface temperature	93.7 K
Diameter	5152 km
Solar flux outside Titan's atmosphere	14.87 W/m^2
Speed of sound at the surface	196.5 m/s
Atmosphere gas constant (R_a)	296.8 J/kg-K
Atmosphere ratio of specific heats (γ_a)	1.4
Atmosphere specific heat (c_{pa})	1039 J/kg-K

TABLE 2.—TITAN ATMOSPHERIC COMPOSITION (REF. 7)

Gas	Percent Volume
Nitrogen (N_2)	94.2%
Methane (CH_4)	5.6%
Hydrogen (H_2)	0.1%
Argon (Ar)	34 ppm

Because of the thick atmosphere, the pressure and density at the surface is greater than that on Earth. The atmospheric pressure on Titan at approximately 8 km altitude is similar to the atmospheric pressure at Earth's surface.

The solar intensity outside the atmosphere is only approximately 15 W/m^2. The low solar intensity coupled with the haze and clouds within the atmosphere make the surface light very dim. This can be a concern for imaging cameras especially on a moving platform where exposure time will be limited.

The winds within the atmosphere blow fairly consistently in the same direction as the planetary rotation (Ref. 5). At altitudes that can be considered for airship operation, below 20 km, the wind speed decreases from approximately 5 m/s to near 0 at the surface.

The gravitational acceleration on Titan (1.35 m/s^2) is less than that of Earth's moon. The atmospheric composition on Titan is mostly nitrogen with a small amount of methane (Ref. 6). The atmospheric composition is given in Table 2. Although, like Earth, the atmosphere is composed mostly of nitrogen, the speed of sound within the atmosphere is about half that on Earth. This is mainly due to the low temperature of the atmosphere compared to Earth's.

The main characteristics of the atmosphere (density, temperature, and wind velocity) are critical in determining the feasibility of airship flight on Titan. These parameters, shown in Figure 3 for an altitude up to 20 km, are provided as functions of altitude (Z) in kilometers by Equations (2.1) to (2.3).

The atmospheric temperature on Titan (T_a in K) decreases fairly linearly from the surface up to approximately 60 km in altitude, as seen in Figure 3. The temperature as a function of altitude in kilometers is approximated by Equation (2.1).

$$T_a = 93.005 - 1.2204Z + 0.024754Z^2 - 0.0003082Z^3 + 2.5861\times10^{-6}\ Z^4 \qquad (2.1)$$

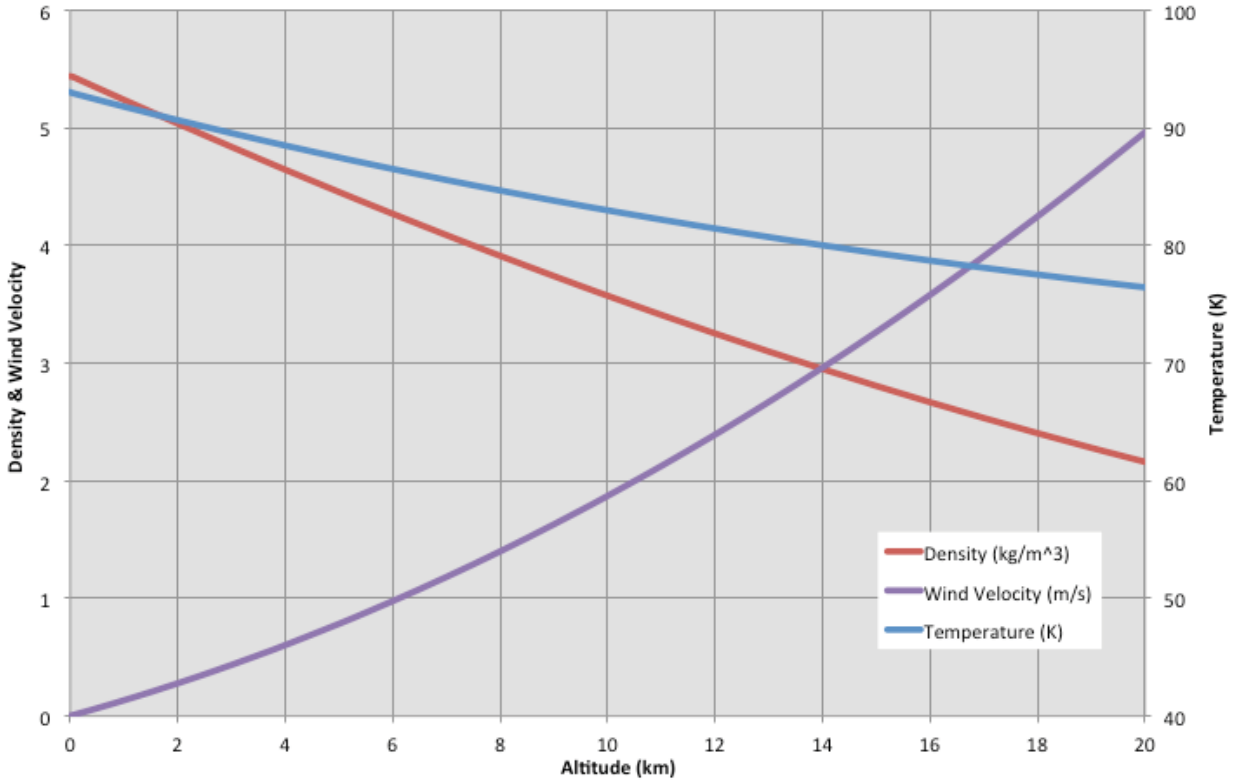

Figure 3.—Temperature, Density and Wind Velocity on Titan (Refs. 4, 5, and 8).

The atmospheric density (ρ_a in kg/m^3) on near the surface on Titan is much greater than that on Earth. It is given by Equation (2.2) as a function of altitude in kilometers.

$$\rho_a = 5.4444 - 0.20758Z + 0.0018503Z^2 - 2.3217\times10^{-5}\ Z^3 - 3.5849\times10^{-7}\ Z^4 \tag{2.2}$$

The average wind speed (v_a in m/s) below 20 km is given by Equation (2.3) as a function of altitude in kilometers.

$$v_a = 0.0023761 + 0.12585Z + 0.0061063Z^2 \tag{2.3}$$

The atmospheric viscosity and thermal conductivity are two additional properties that are critical in evaluating the airship operation. Since the atmosphere is composed mainly of nitrogen, the viscosity and thermal conductivity of nitrogen was used (Ref. 9). The atmospheric viscosity (μ_a in kg/m-s) as a function of the atmosphere temperature and density is given by Equations (2.4) to (2.10) (Ref. 7).

$$\mu_a = \left(\frac{1.057\sqrt{T_a}}{C_1} + C_2 + C_3 + C_4 + C_5 + C_6\right)10^{-6} \tag{2.4}$$

$$C_1 = e^{\left[0.431 - 0.4623\ln\left(\frac{T_a}{98.94}\right) + 0.0846\left[\ln\left(\frac{T_a}{98.94}\right)\right]^2 + 0.005341\left[\ln\left(\frac{T_a}{98.94}\right)\right]^3 - 0.00331\left[\ln\left(\frac{T_a}{98.94}\right)\right]^4\right]} \tag{2.5}$$

$$C_2 = 1.7728\times10^{-4}\frac{\rho_a^2}{T_a^{0.1}} \tag{2.6}$$

$$C_3 = 1.472 \times 10^{-26} \frac{\rho_a^{10}}{T_a^{0.25}} e^{-\frac{\rho_a}{313.19}} \tag{2.7}$$

$$C_4 = 7.1726 \times 10^{-27} \frac{\rho_a^{12}}{T_a^{3.2}} e^{-\frac{\rho_a}{313.19}} \tag{2.8}$$

$$C_5 = -0.00587^{-27} \frac{\rho_a^{2}}{T_a^{0.09}} e^{-\left(\frac{\rho_a}{313.19}\right)^2} \tag{2.9}$$

$$C_6 = 0.062971 \frac{\rho_a}{T_a^{0.3}} e^{-\left(\frac{\rho_a}{313.19}\right)^3} \tag{2.10}$$

The atmospheric thermal conductivity (k_a in W/mK) as a function of the atmosphere temperature and density is given by Equations (2.11) to (2.16) (Ref. 9).

$$k_a = \left(\frac{1.597\sqrt{T_a}}{C_1} + 0.0168 T_a - 2.375 T_a^{0.07} + C_7 + C_8 + C_9 + C_{10} + C_{11} \right) 10^{-3} \tag{2.11}$$

$$C_7 = 0.028\rho_a + 3.6671 \times 10^{-4} \frac{\rho_a^2}{T_a^{0.3}} \tag{2.12}$$

$$C_8 = -6.264 \times 10^{-6} \frac{\rho_a^3}{T_a^{0.2}} e^{\frac{\rho_a}{313.19}} \tag{2.13}$$

$$C_9 = 99.833 \times 10^{-9} \frac{\rho_a^4}{T_a^{0.8}} e^{\left(\frac{\rho_a}{313.19}\right)^2} \tag{2.14}$$

$$C_{10} = 1.3969 \times 10^{-19} \frac{\rho_a^8}{T_a^{0.6}} e^{\left(\frac{\rho_a}{313.19}\right)^2} \tag{2.15}$$

$$C_{11} = 2.888 \times 10^{-22} \frac{\rho_a^{10}}{T_a^{1.9}} e^{\left(\frac{\rho_a}{313.19}\right)^2} \tag{2.16}$$

The last atmospheric property that will be needed to evaluate the airship is the speed of sound within the atmosphere (a in m/s). This is given by Equation (2.17).

$$a = \sqrt{\gamma_a R_a T_a} \tag{2.17}$$

3.0 Airship Configuration and Sizing

For flight on Titan the airship is configured similarly to a standard airship that would operate on Earth. The envelope is ellipsoidal with rear fins for stability and control. The equipment and payload are housed in an elliptical shaped insulated enclosure. An electric motor and propeller are used for propulsion and a radioisotope power Stirling engine is used to provide electrical power to operate the onboard equipment, run internal heaters and provide power to the propulsion system. This general layout is shown in Figure 4.

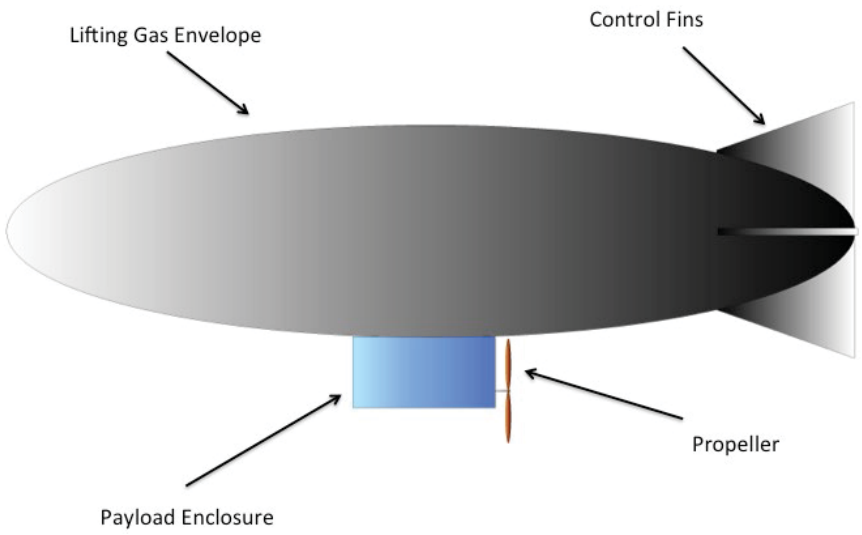

Figure 4.—Titan Airship Main Component layout.

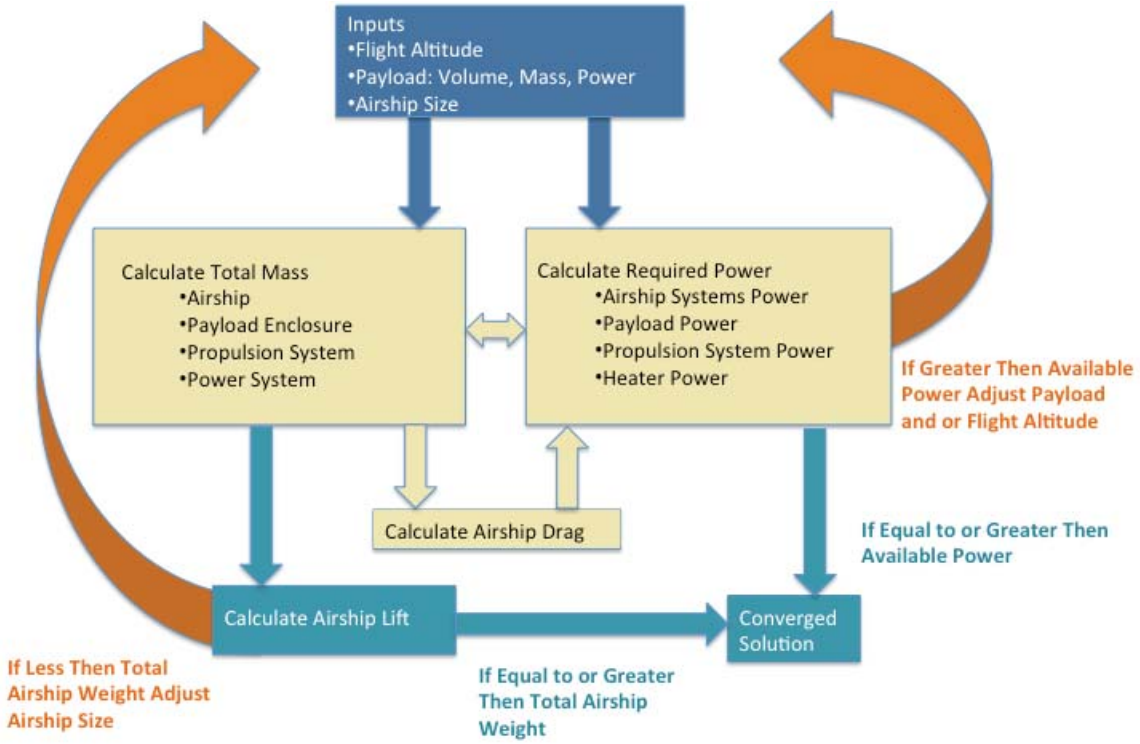

Figure 5.—Logic diagram for airship sizing analysis.

Sizing the airship for flight on Titan is an iterative process based on the desired flight altitude and speed. The component masses and sizes are calculated from an initial guess at the required lift and power needed for the airship to operate. From these the actual lift and power requirements are determined. These are compared against the estimated values. If different, then the vehicle size is adjusted and the mass, lift and power is recalculated. This iterative process is continued until the initial and calculated lift and power values converge. A converged solution represents a design point for the vehicle that meets the selected flight environment and payload requirements. This airship sizing method is illustrated in Figure 5.

TABLE 3.—SCALING AND EFFECT DEPENDENCE OF AIRSHIP COMPONENTS

Component	Scaling factor	Effect on airship
Airship Structure: Envelope, tail, structural supports, lifting gas	Airship geometry and size, flight speed, altitude	Lifting capability, drag, mass
Propulsion Drive Train: Electric motor, motor controller, gearbox, power conditioning, propeller	Propulsion Power and Thrust, Flight Speed, Altitude	Power consumption, flight velocity, mass
Stirling Engine System: (ASRG)	Number of ASRG systems, flight speed, altitude	Power availability, mass
Payload and Electronics: Flight control computer, communications equipment, payload, sensors	Variables, constants	Power consumption, mass
Payload/Electronics Enclosure: Insulation, view port, sensor feed through	Interior volume and temperature	Mass and cooling power

3.1 Airship Mass

The total airship mass is the sum of all the components and systems that make up the airship. These components are scaled based on various factors such as power level, size, velocity, altitude, etc. The components and their associated scaling factors are listed in Table 3.

3.1.1 Structure Mass

The airship shape is assumed to be an ellipsoid with its length going from the front tip to the rear tip and the diameter being the maximum thickness in the center of the airship. The fineness ratio of the airship is the ratio of length to diameter. The length and fineness ratio are used as the input variables to vary the airship size and geometry.

The airship structure mass (m_s) is based on the aerial density (assumed to be 0.25 kg/m^2) of the covering, the number of control fins and ratio of fin area to airship volume along with a fin structure factor (assumed to be 1.2) to account to the internal structural support and controls for the fins. In addition a structure factor assumes that the internal structure of the airship envelope scales as 1/4 of the total mass of the airship (Ref. 10) (m_{tot}). This component is added to account for the fixed structure needed to attach components to the envelope.

Details on the calculation of the airship structure mass are given in Reference 11.

3.1.2 Propulsion System Mass

The propulsion system mass consists of the mass of the electric motor, motor controller, gearbox, propulsion power conditioning electronics and propeller. The operational efficiency of each of the components of the power system must also be taken into account when sizing the airship. The airship power train is shown in Figure 6. The total efficiency of the propulsion system drive train is composed of the motor controller efficiency electric motor efficiency gearbox efficiency power conditioning efficiency and propeller efficiency. They are combined to get the driveline efficiency, which consists of all components up to the propeller. The propeller efficiency has to be calculated based on a propeller sizing for the operational altitude and thrust requirement. These efficiencies are representative approximations for each of the components under optimized operating conditions. Details on the drive train efficiencies are given in Reference 11.

The electric motor mass, motor controller mass, gearbox mass, and mass of the power conditioning system is based on a linear scaling with power output (P_{dt}) (Refs. 11, 12, and 13). The propeller mass is based on the propeller diameter and the number of blades. The diameter is dependent on the amount of thrust generated by the propeller. This thrust will be equal to the airship drag (D_{tot}) at the desired flight speed. With the diameter and number of blades known, the mass of the propeller will depend on the volume of each blade, its material density, and the void fraction within the blade. For a given airfoil cross-sectional area and the chord length distribution the volume of the propeller blade can be calculated. An initial trade off was performed on the number of propeller blades to utilize. For the environmental conditions on Titan a four bladed propeller was chosen. The propeller blades would be constructed of carbon composite, with a density of 1380 kg/m^3, and with no void space within the blade. Also a 10 percent increase in the total propeller blade mass was added to account for the hub and attachment to

the drive shaft. The total propulsion system drive train mass (m_{dt}) is the sum of the masses of all the components shown in Figure 4. Additional details on the mass calculation for the drive train components are given in Reference 11.

3.1.3 Power System Mass

The baseline power generation system consists of two advanced Stirling radioisotope generators (ASRG). They provide electrical power to the drive motor as well as to the electronics, payload and heaters. The ASRG, illustrated in Figure 7, generates electrical power through a Stirling engine operating off of two plutonium-238, general purpose heat source (GPHS) blocks. The system shown in Figure 7 is a typical arrangement for a space mission. Two of the systems shown in Figure 7 will be used for powering the baseline Titan airship. The mass of each ASRG power system (m_{asrg}) is estimated at 25 kg (Ref. 14).

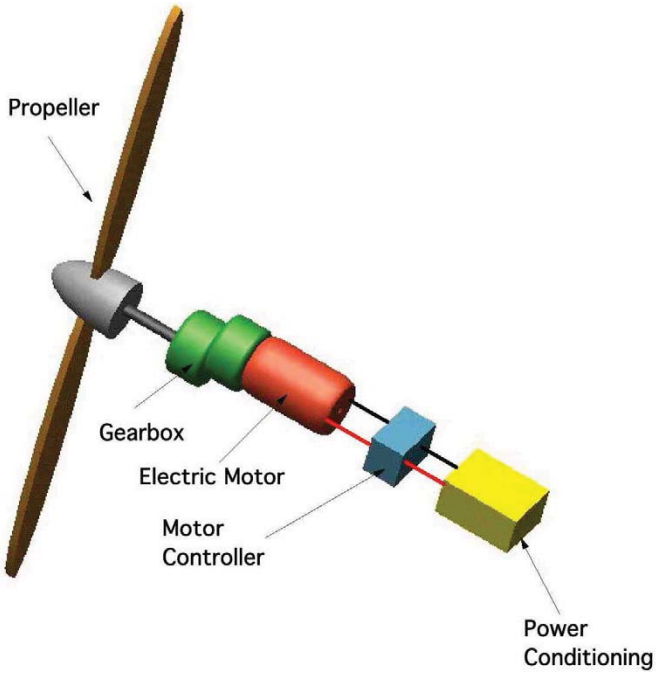

Figure 6.—Propulsion System component layout.

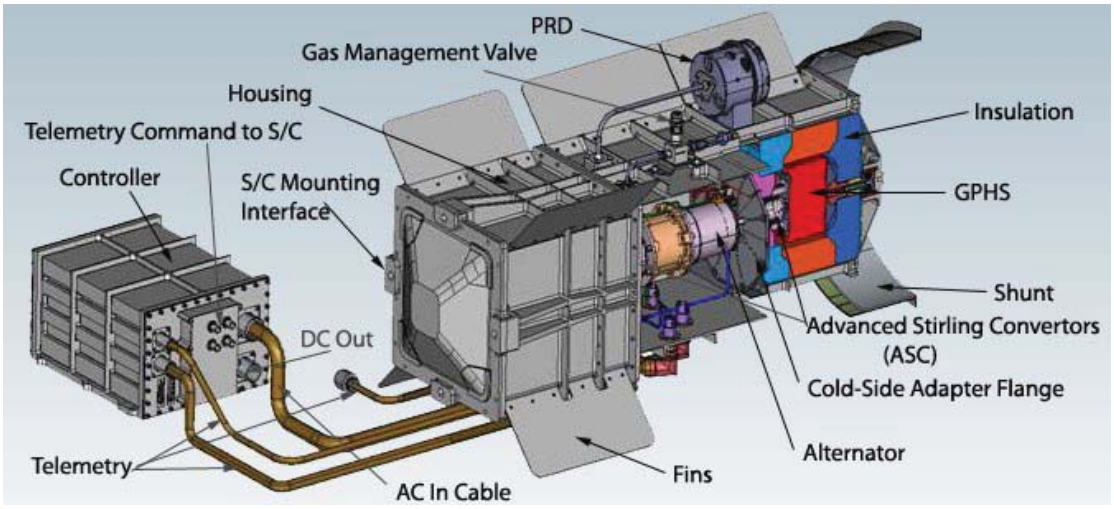

Figure 7.—ASRG typical arrangement and components (Ref. 15).

3.1.4 Payload Enclosure Mass

The payload enclosure is used to house the ASRG power sources, avionics, electronics and science payload. It is composed of an inner and outer wall constructed of carbon composite with aerogel insulation between the walls. The enclosure operates at the ambient pressure and with ambient atmospheric gas within the chamber. The layout of the payload enclosure is shown in Figure 8. The enclosure is separated into two sections, the upper section houses the ASRGs and the lower section houses the remaining equipment. This was done due to the different ambient temperature operating requirements between the ASRG and the other equipment.

Because the atmosphere is composed mainly of nitrogen without any corrosive trace gasses it is fairly inert and capable of being utilized within the enclosure. This along with operating at atmospheric pressure provides a number of benefits to the system design which include:

- The chamber can be vented so that it would not be required to maintain a pressure differential through the different phases of the mission (Earth ground operations, launch, spaceflight and operation on Titan).
- The structure mass is minimized by eliminating the need for pressurization during the mission.
- Lightweight aerogel can be utilized as the interior insulation.
- Internal convection can be used to evenly distribute the internal heating.
- Enables easier atmospheric sampling and testing.

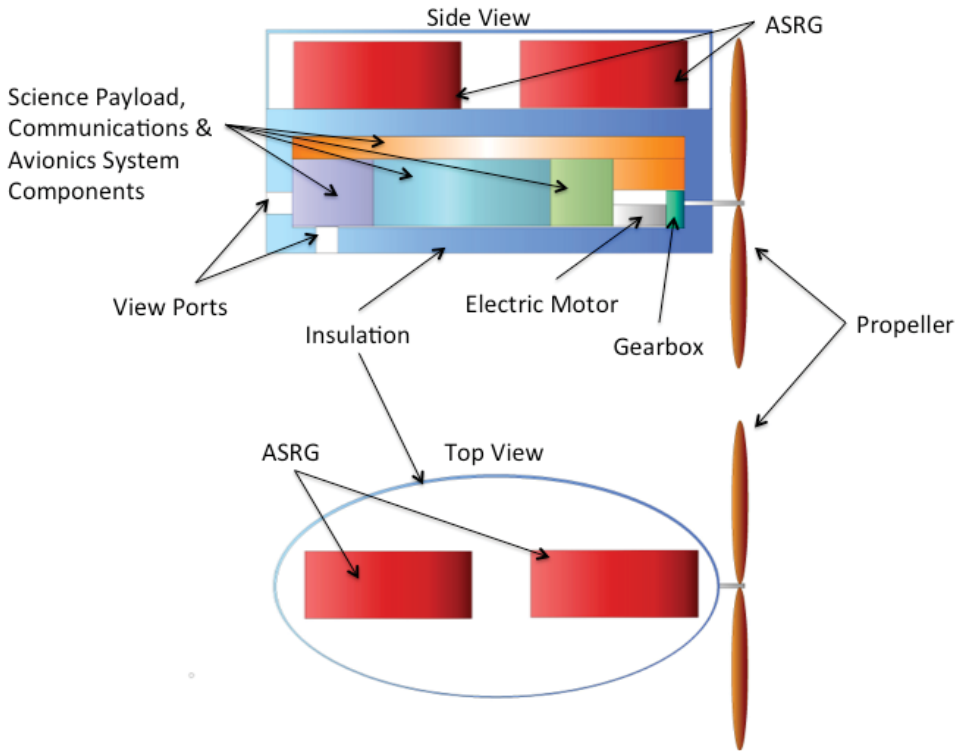

Figure 8.—Payload enclosure layout.

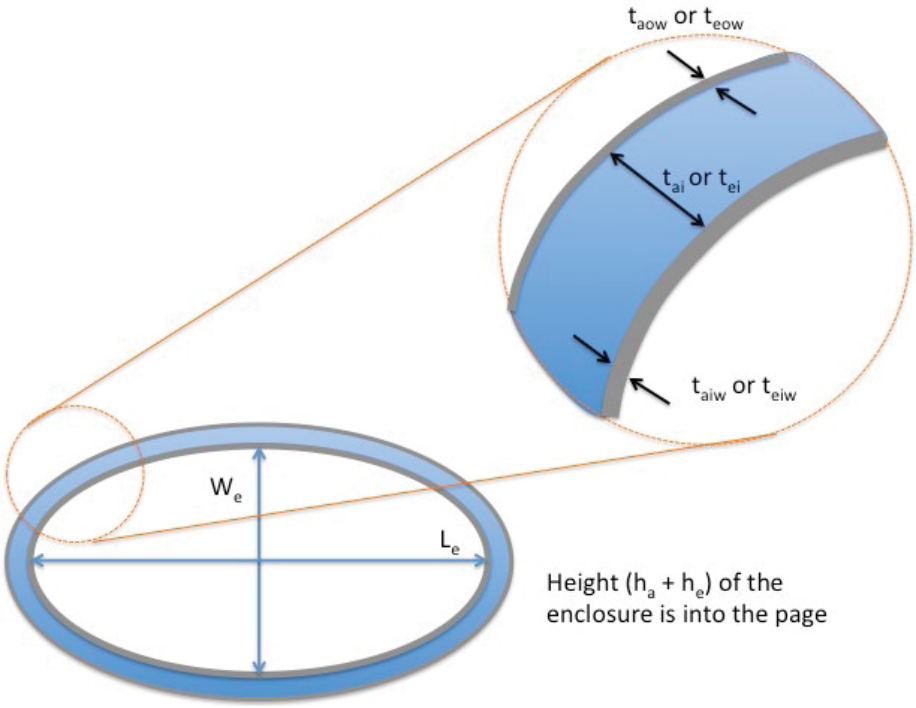

Figure 9.—Pressure vessel structure and insulation layout.

The mass of each layer of the payload enclosure is based on its thickness, surface area and material density. These are illustrated in Figure 9. The outer shell wall (thickness t_{aow} and t_{eow}) is mainly structural and is used to maintain the aerodynamic shape of the enclosure and resist aerodynamic loads. The inner wall is the main structural element of the payload enclosure. It is used to support the payload components. Between the inner and outer wall is the insulation. Its thickness determines the separation distance between the two structural walls. Because of the different temperature requirements the insulation thickness will vary between the portion of the enclosure containing the ASRG power systems and the lower section containing the electronics and other systems. However the outside dimensions of both sections are the same to provide a smooth continuous surface on the exterior of the enclosure in order to reduce aerodynamic drag.

Therefore, mass of each layer of the enclosure is based on the electronics portion interior dimensions (length L_e, width W_e and height h_e) and the thickness of the wall for each layer. To determine the mass of each layer, the perimeter for each layer is calculated at the center of the layer or half its thickness. The layer perimeter (p_i) is given in general form by Equations (3.1) and (3.2). The layer thickness variables used to determine the perimeter for a specific layer and section of the enclosure is given in Table 4.

$$p_i = \pi\left(\frac{L_e + W_e}{2} + d_i\right)\left(1 + \frac{c_i}{4} + \frac{(c_i)^2}{64} + \frac{(c_i)^3}{256}\right) \tag{3.1}$$

$$c_i = \frac{\left(\frac{L_e + d_i}{2} - \frac{W_e + d_i}{2}\right)^2}{\left(\frac{L_e + d_i}{2} + \frac{W_e + d_i}{2}\right)^2} \tag{3.2}$$

TABLE 4—MASS VARIABLES FOR THE DIFFERENT LAYERS FOR EACH PERIMETER WALL SECTION OF THE PAYLOAD ENCLOSURE

Location		Section height (h_i)	Perimeter variable (p_i)	Layer thickness (t_{pwi})	Incremental thickness (d_i)	Layer material density (ρ_{pwi})	Layer mass variable (m_{pwi})
ASRG section	Inner wall	h_a	p_{aiw}	t_{aiw}	$t_{eiw} + t_{ie} + t_{eow} - t_{aow} - t_{ai}$	ρ_{aiw}	m_{aiw}
	Insulation		p_{ai}	t_{ai}	$t_{eiw} + t_{ie} + t_{eow} - t_{aow}$	ρ_{ai}	m_{ai}
	Outer		p_{aow}	t_{aow}	$t_{eiw} + t_{ie} + t_{eow}$	ρ_{aow}	m_{aow}
Electronic/ payload section	Inner wall	h_e	p_{eiw}	t_{eiw}	t_{eiw}	ρ_{eiw}	m_{eiw}
	Insulation		p_{ei}	t_{ei}	$t_{eiw} + t_{ei}$	ρ_{ei}	m_{ei}
	Outer		p_{eow}	t_{eow}	$t_{eiw} + t_{ei} + t_{eow}$	ρ_{eow}	m_{eow}

The mass for each layer of the perimeter walls (m_{pwi}) can then be calculated based on the corresponding perimeter (p_i) value given by Equations (3.1) and (3.2). The mass is also dependent on the height of each section (h_i) of the enclosure and the density of the material utilized (ρ_{pwi}). The general mass equation for each of the layers is given by Equation (3.3). By inserting the variables listed in Table 4, the corresponding mass of each layer of both sections can be determined.

$$m_{pwi} = p_i h_i t_{pwi} \rho_{pwi} \tag{3.3}$$

The total mass of the outer elliptical walls of the payload enclosure (m_{pw}) is the sum of the individual layer masses given in Table 4, as given by Equation (3.4).

$$m_{pw} = m_{aiw} + m_{ai} + m_{aow} + m_{eiw} + m_{ei} + m_{eow} \tag{3.4}$$

The payload enclosure also has an insulated lower and upper end cap and an insulated deck separating the ASRG compartment from the electronics and payload compartment.

These end layers are constructed in the same fashion as the outer elliptical walls. There is an upper wall, insulation and lower wall. The mass of the horizontal wall layers (m_{hwi}) is given by Equation (3.5) and the variables for each layer of the three walls are given in Table 5.

$$m_{hwi} = \pi \frac{W_e L_e t_{hwi} \rho_{hwi}}{4} \tag{3.5}$$

As with the outer perimeter walls, the total mass of the horizontal walls (m_{hw}) is the sum of the individual layers of each wall, as given by Equation (3.6).

$$m_{hw} = m_{uiw} + m_{ui} + m_{uow} + m_{muw} + m_{mi} + m_{mlw} + m_{liw} + m_{li} + m_{low} \tag{3.6}$$

The total mass of the payload enclosure (m_{pe}), given by Equation (3.7), is the sum of the masses of the perimeter walls and horizontal walls represented by Equations (3.5) and (3.6), respectively. An additional 10 percent margin is added to the total mass to account for items such as internal structure and miscellaneous hardware.

$$m_{pe} = \left(m_{pw} + m_{hw}\right) 1.1 \tag{3.7}$$

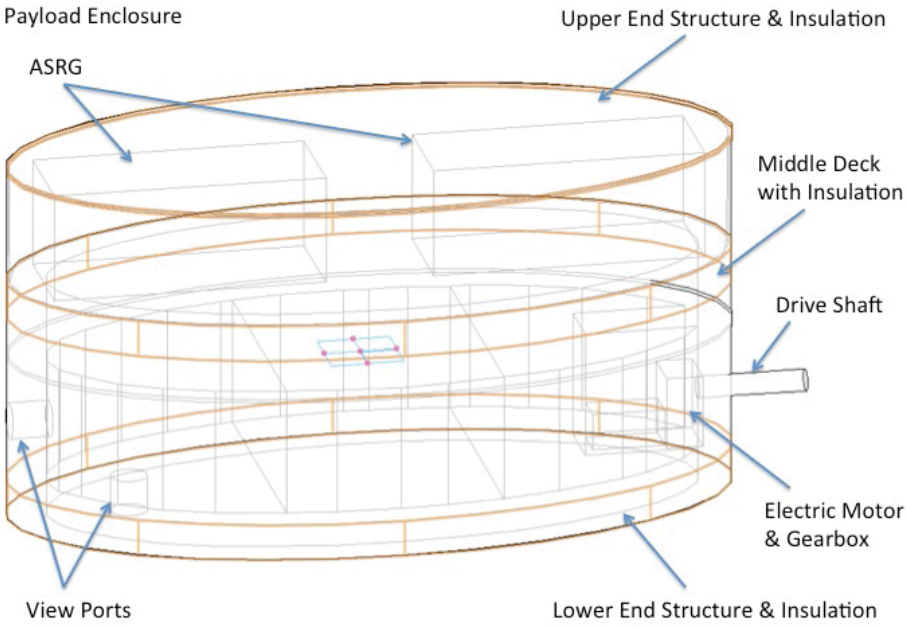

Figure 10.—Insulated structural layers within the payload enclosure.

TABLE 5.—MASS VARIABLES FOR THE DIFFERENT LAYERS FOR EACH HORIZONTAL WALL SECTION OF THE PAYLOAD ENCLOSURE

Location		Layer thickness (t_{hwi})	Layer material density (ρ_{hwi})	Layer mass variable (m_{hwi})
Upper end	Inner wall	t_{uiw}	ρ_{uiw}	m_{uiw}
	Insulation	t_{ui}	ρ_{ui}	m_{ui}
	Outer	t_{uow}	ρ_{uow}	m_{uow}
Middle deck	Upper wall	t_{muw}	ρ_{muw}	m_{muw}
	Insulation	t_{mi}	ρ_{mi}	m_{mi}
	Lower wall	t_{mlw}	ρ_{mlw}	m_{mlw}
Lower end	Inner wall	t_{liw}	ρ_{liw}	m_{liw}
	Insulation	t_{li}	ρ_{li}	m_{li}
	Outer	t_{low}	ρ_{low}	m_{low}

3.1.5 Lifting Gas Mass

The airship shape determines the available internal volume for the lifting gas. It is assumed to be an ellipsoid with its length (l) going from the front tip to the rear tip and the diameter (d) being the maximum thickness in the center of the airship. The fineness ratio (f) of the airship is the ratio of length to diameter as given by Equation (3.8). The length and fineness ratio are used as the input variables to vary the airship size and geometry. The corresponding lifting gas volume (V_a) is given by Equation (3.9).

$$f = \frac{l}{d} \tag{3.8}$$

$$V_a = \frac{4\pi l^3}{3f} \tag{3.9}$$

The lifting gas mass (m_{lg}) also factors into the total airship mass. Its mass is dependent on the lifting gas molecular weight (M_{Wg}), atmospheric temperature and pressure (P_a) and the airship gas volume (V_a), as given by Equations (3.10) and (3.11). Where the universal gas constant (R) has a value of 0.0831 m^3Bar/kMol K and it is assumed the lifting gas is at atmospheric conditions.

$$P_a = \rho_a R_a T_a \tag{3.10}$$

$$m_{1g} = \frac{M_{Wg} V_a P_a}{T_a R} \tag{3.11}$$

3.1.6 Total Mass

The last series of components that have to be accounted for in determining the total mass of the airship are fixed and do not scale with the airship size. These fixed mass components are listed in Table 6.

The sum of these fixed mass items is given by Equation (3.12).

$$m_{fi} = m_{fc} + m_{ce} + m_{fs} + m_{pl} \tag{3.12}$$

From the above equations the total airship mass (m_{tot}), given by Equation (3.13), can be calculated.

$$m_{tot} = m_s + m_{dt} + m_{asrg} + m_{pe} + m_{lg} + m_{fi} \tag{3.13}$$

3.2 Lift Generation

Determining the total airship mass and subsequent gas envelope size is an iterative process. The airship envelope volume determines the total weight that the airship can lift. The lifting force (L) of the airship is based on a centuries old principle discovered by Archimedes, "A body wholly or partly immersed in a fluid is buoyed up with a force equal to the weight of the fluid displaced by the body". This principle is expressed by Equation (3.14), which is dependent on the gravitational force on Titan (g =1.35 m/s^2), the ratio of the molecular weights of the lifting gas and the atmosphere (M_{Wa}), the density of the atmosphere and the gas constant of the atmosphere (Ra = 296.8 J/kg-K). This equation assumes that the pressure within the lifting gas envelope is the same as that of the atmosphere and unless the lifting gas is actively heated, its temperature (T_g) will also be the same as that of the atmosphere.

$$L = \left[\rho_a V_a \left(1 - \frac{M_{Wg} T_a}{M_{Wa} T_g} \right) \right] g \tag{3.14}$$

TABLE 6.—AIRSHIP FIXED COMPONENT MASSES

Component	Mass (kg)	Power (W)
Flight control computer (m_{fc}, P_{fc})	3.8	25
Communications equipment (m_{ce}, P_{ce})	4.6	50
Flight control sensors (m_{fs}, P_{fs})	3.5	25
Payload (m_{pl}, P_{pl})	25.0	50

The total lifting force is then compared to the total weight of the airship (W_{tot}), as given by Equation (3.15). In the analysis the envelope size is then iterated on until the lifting force is greater than or equal to the airship weight.

$$W_{tot} = gm_{tot} \tag{3.15}$$

3.3 Power Required

The next step in sizing the airship is determining the total power required to fly and operate the airship and payload systems. Determining this is an iterative process between the sizing of the airship to lift its mass and the propulsion system power needed to overcome drag due to its size and shape along with the power needed to provide heating to the payload enclosure and operate the airship systems and payload. As with the total mass, the total required power (P_r) will be a summation of the power required by the various systems of the airship given by Equation (3.16). The power consuming items, on the airship include the propulsion system (P_{dt}), payload enclosure heating (P_h) and sensors/payload, communications and control. These items are listed in Table 6.

$$P_r = P_{dt} + P_h + P_{fc} + P_{ce} + P_{fs} + P_{pl} \tag{3.16}$$

3.3.1 Propulsion Power

The propulsion power required by the airship to fly at a specified velocity (U) is dependent on the total airship drag (D_{tot}) and the propulsion system efficiency (η_{dt}) as given by Equation (3.17).

$$P_{dt} = \frac{D_{tot}U}{\eta_{dt}} \tag{3.17}$$

The total airship drag is the summation of the drag of each component exposed to the atmosphere flow over the airship as it moves. The main airship structure containing the lifting gas can be broken into two segments, the gas envelope and the tail section with control fins. The lifting gas envelope drag (D_e), given by Equation (3.18) is based on the airship's velocity, the volume of the lifting gas and its drag coefficient (c_{de}).

$$D_e = \frac{1}{2}\rho_a U^2 c_{de} V_a^{\frac{2}{3}} \tag{3.18}$$

The gas envelope drag coefficient is based on the fineness ration for the airship and is given by Equation (3.19). This equation represents a curve fit to drag coefficient data for various airship fineness ratios (Ref. 10).

$$c_{de} = 0.2318 - 0.1576f + 0.04744f^2 - 0.007041f^3 + 5.135\times10^4 f^4 - 1.48\times10^5 f^5 \tag{3.19}$$

The tail section drag (D_t) is scaled linearly from the lifting gas envelope drag as given by Equation (3.20) (Ref. 10).

$$D_t = 0.167D_e \tag{3.20}$$

The next main drag is for the payload enclosure. The payload enclosure is mounted on the bottom of the elliptical lifting gas envelope. The enclosure is symmetrical with an elliptical cross-section, as shown in Figure 10.

The main payload enclosure drag (D_p) is given by Equation (3.21). The drag coefficient (c_{dp}) for the payload enclosure is approximated from empirical data (Ref. 16) as a function of Reynolds number (Re_p) by Equations (3.22) and (3.23).

$$D_p = 0.5\rho_a c_{dp} U^2 \left(W_e + 2\left(t_{eow} + t_{ei} + t_{eiw}\right)\right)\left(h_a + h_e\right) \tag{3.21}$$

$$c_{dp} = 0.7 - 6.3\times10^{-7}\,\mathrm{Re}_p + 1.97\times10^{-13}\,\mathrm{Re}_p^2 - 1.74\times10^{-20}\,\mathrm{Re}_p^3 \tag{3.22}$$

$$\mathrm{Re}_p = \frac{\rho_a U\left(L_e + 2\left(t_{eow} + t_{ei} + t_{eiw}\right)\right)}{\mu_a} \tag{3.23}$$

From these components the total drag for the airship can be determined, as given by Equation (3.24).

$$D_{tot} = D_e + D_t + D_p \tag{3.24}$$

3.3.2 Heating Power

The heating power for maintaining the desired operating temperature for the electronics/payload enclosure is the largest power-consuming item. The required heating power is dependent on the heat loss through the payload enclosure to the surroundings. The required heater power is based on the heat loss from the following sources.

- Through the insulation and enclosure walls to the atmosphere (Q_i)
- Through the insulation to the ASRG portion of the enclosure (Q_a)
- Wire and cable pass-through for the sensors through the insulation to the atmosphere (Q_{pt})
- Through the view port windows to the atmosphere (Q_{vp})

The power consumed by the internal electronics and payload is eventually turned into heat therefore it is subtracted from the total required heater power.

$$P_h = Q_i + Q_a + Q_{pt} + Q_{vp} - P_{fc} - P_{pl} \tag{3.25}$$

The heat loss through the insulation to the atmosphere is based on the temperature difference between the interior (T_{ie}) and exterior, the thermal resistance of the materials that make up the walls and the thermal resistances associated with the natural convection within the payload enclosure and the convection from its exterior. The equations for heat loss through the insulation in the electronics and payload portion of the payload enclosure to the atmosphere is given by Equations (3.26) to (3.30).

$$Q_i = \frac{T_a - T_{ie}}{R_{eiw} + R_{ei} + R_{eow} + R_{eic} + R_{oc}} \tag{3.26}$$

The thermal resistance (R_t) terms for the different material layers that comprise the payload enclosure are all similar and are based on the surface area (A_{lp}) of the layers as well as the thickness (t_{pwi}) of the layer and its thermal conductivity (k_p), as given by Equation (3.27).

$$R_t = \frac{t_{pwi}}{k_p A_{lp}} \tag{3.27}$$

For the elliptical shape of the payload enclosure, the surface area is dependent on the outer perimeter for that layer, the height of the payload section and the bottom surface area of the enclosure as given by Equation (3.28).

$$A_{lp} = p_i h_i + \pi \frac{L_e W_e}{4} \tag{3.28}$$

The perimeter for each layer is determined from Equations (3.1) and (3.2).

Heat is also lost from the electronics and payload portion of the enclosure to the ASRG portion of the enclosure since it is held at a much lower temperature (T_{ia}). This heat loss is given by Equation (3.29).

$$Q_a = \frac{T_{ia} - T_{ie}}{R_{muw} + R_{mi} + R_{mlw} + R_{eic} + R_{aic}} \tag{3.29}$$

The thermal resistances for the layers between the two sections of the payload enclosure are also given by Equation (3.28) where the first term is zero.

For the separation between the two sections of the payload enclosure the surface area is the same for each layer. The variables, used for the corresponding thermal resistance variables for each of the layers within the payload enclosure, in Equations (3.26) to (3.29), are given in Table 7.

The remaining three resistance terms from Equations (3.26) and (3.29) are due to the internal and external convection within the electronics section of the payload enclosure (R_{eic}), within the ASRG section of the payload enclosure (R_{aic}) and outside (R_{oc}) to the atmosphere from the electronics portion of the payload enclosure. The convective resistance terms are given by Equations (3.30) to (3.32), respectively. These thermal resistances are dependent on the internal convection coefficients for the electronics (h_{ei}) and ASRG sections (h_{ai}) of the enclosure and the external convection coefficient (h_o) outside the enclosure.

$$R_{eic} = \frac{1}{h_{ei} A_{eiw}} \tag{3.30}$$

$$R_{aic} = \frac{1}{h_{ai} A_{la}} \tag{3.31}$$

$$R_{oc} = \frac{1}{h_o A_{eow}} \tag{3.32}$$

TABLE 7.—THERMAL RESISTANCE VALUES AND THEIR CORRESPONDING VARIABLES

Resistance term (R_t)	Thermal conductivity (k_p)	Layer area (A_{lp})	Perimeter (p_i)	Layer thickness (t_{pwi})	Incremental thickness (d_i)
Electronics section inner wall (R_{eiw})	k_{eiw}	A_{eiw}	p_{eiw}	t_{eiw}	t_{eiw}
Electronics section insulation layer (R_{ei})	k_{ei}	A_{ei}	P_{ei}	t_{ei}	$t_{eiw} + t_{ei}$
Electronics section outer wall (R_{eow})	k_{eow}	A_{eow}	p_{eow}	t_{eow}	$t_{eiw} + t_{ei} + t_{eow}$
ASRG/payload separation inner wall (R_{muw})	k_{muw}	A_{la}	0	t_{muw}	N/A
ASRG/payload separation insulation layer (R_{mi})	k_{mi}	A_{la}	0	t_{mi}	N/A
ASRG/payload separation outer wall (R_{mlw})	k_{mlw}	A_{la}	0	t_{mlw}	N/A

Determining the convection coefficients for each of the convection thermal resistance terms is a key aspect in accurately calculating the heat leak through the walls and insulation of the payload enclosure. The interior convection coefficients for the electronics and ASRG sections of payload enclosure are given by Equations (3.33) and (3.34), respectively. The convection coefficient for the exterior surfaces is given by Equation (3.35). These coefficients are determined by utilizing the geometry and atmospheric gas properties calculated for the conditions at each location. The main factor in calculating the convective coefficients is in determining the Nusselt number (Nu_{di} and Nu_{do}) for each location.

$$h_{ei} = \frac{k_a \mathrm{Nu}_{di}}{h_e} \tag{3.33}$$

$$h_{ai} = \frac{k_a \mathrm{Nu}_{di}}{h_a} \tag{3.34}$$

$$h_o = \frac{k_a \mathrm{Nu}_{do}}{L_e + t_{eiw} + t_{ei} + t_{eow}} \tag{3.35}$$

For calculating the internal convective coefficient the interior is filled with atmospheric gas at atmospheric pressure. The thermal conductivity for this gas (k_a) is given by Equation (2.11), calculated at the gas temperature for the section in which the coefficient is being determined as given in Table 8. The internal convective heat transfer is assumed to be free convection with no active mixing of the gas within the enclosure. Therefore there will be a boundary layer with a temperature gradient between the interior wall and the internal gas. The film layer temperature is the average of the interior temperature and the wall temperature. The difference between the wall and the interior gas temperature (ΔT_{wi}) was assumed to be 10 °C.

The Nusselt number (Nu_{di}) for internal free convection within the payload enclosure is given by Equation (3.36) (Ref. 17).

$$\mathrm{Nu}_{di} = 0.18\left(\frac{\mathrm{Pr}_i \, \mathrm{Ra}_i}{0.2 + \mathrm{Pr}_i}\right)^{0.29} \tag{3.36}$$

The payload enclosure internal gas Prandtl number (Pr_i) is based on the internal gas specific heat, thermal conductivity and dynamic viscosity (μ_a), calculated for the temperature and gas density within each section of the payload enclosure, as defined by Equation (3.37).

$$\mathrm{Pr}_i = \frac{c_{pa} \mu_a}{k_a} \tag{3.37}$$

To calculate the Prandlt number for the internal gas the thermal conductivity is given by Equation (2.11), using the temperature listed in Table 8 for the appropriate section within the payload enclosure. The specific heat for the atmosphere is 1039 J/kg-K and the dynamic viscosity is given by Equation (2.4).

TABLE 8—TEMPERATURE FOR CALCULATING THE GAS THERMAL CONDUCTIVITY AT DIFFERENT LOCATIONS ON THE PAYLOAD ENCLOSURE

Location	Temperature
Internal walls of the electronics portion of the payload enclosure	$T_{ie} - \Delta T_{wi}/2$
Internal walls of the ASRG portion of the payload enclosure	$T_{ia} - \Delta T_{wi}/2$
External walls of the payload enclosure	T_a

The last factor in calculating the Nusselt number is the determination of the Rayleigh number for the payload enclosure internal gas (Ra_i), defined in Equation (3.38). The Rayleigh number is based on the interior wall film temperature (T_{if}), the kinematic viscosity (ν_a, given by Eq. (3.39)) and the thermal diffusivity (α_a, given by Eq. (3.40)) of the atmospheric gas at the internal conditions for each section of the payload enclosure.

$$\mathrm{Ra}_i = \frac{g\Delta T_{wi} h_i^3}{T_{if}\nu_a\alpha_a} \tag{3.38}$$

$$\nu_a = \frac{\mu_a}{\rho_a} \ \{\mathrm{m}^2/\mathrm{s}\} \tag{3.39}$$

$$\alpha_a = -2.13\times10^{-6} + 2.51\times10^{-8} T_{if} + 1.84\times10^{-10} T_{if}^2 \ \{\mathrm{m}^2/\mathrm{s}\} \tag{3.40}$$

The convective coefficient for the flow over the exterior of the pressure vessel is given by Equation (3.35). Unlike the interior, the convective heat transfer for the flow over the exterior of the pressure vessel is forced convection. Therefore, the Nusselt number calculation will be different than that for the interior. Calculating the Nusselt number for the exterior flow is somewhat difficult due to the very high Reynolds number of the flow over the exterior of the sphere.

At flight speeds near the wind velocity of 2 m/s the Reynolds number, as given by Equation (3.20), is on the order of 3 million. There were no available correlations found for the Nusselt number for flow over an elliptical cylinder at a Reynolds number in this range. Therefore a correlation for flow over a cylinder was used as an approximation. Equation (3.41) represents the Nusselt number as a function of Reynolds number for a cylinder in a cross-flow (Ref. 17). This equation is valid for the product of Prandtl and Reynolds numbers greater than 0.2 ($\mathrm{PrRe}_d > 0.2$).

$$\mathrm{Nu}_{do} = 0.3 + \frac{0.62\,\mathrm{Re}_{do}^{0.5}\,\mathrm{Pr}^{1/3}}{\left[1+\left(\frac{0.4}{\mathrm{Pr}}\right)^{2/3}\right]^{0.25}}\left[1+\left(\frac{\mathrm{Re}_{do}}{282000}\right)^{0.625}\right]^{0.8} \tag{3.41}$$

With this expression for Nusselt number, the convective coefficient for the atmosphere flow around the payload enclosure, given by Equation (3.35), can be calculated and in turn the exterior convective resistance term, given by Equation (3.33).

The heaters will not only need to provide heat to make up for the heat leaking in through the insulation, but also the wires and view port as well. The heat leak through the pass-through wires and view port windows (Q_{pt} and Q_{vp} respectively) is depending on the number of wires (n_w) and view ports (n_{vp}), their diameter (d_w, d_{vp}) and the thermal conductivity of the wire (k_w) or viewport (k_{vp}). The heat leak through the wires and view ports is given by Equations (3.42) and (3.43), respectively.

$$Q_{pt} = \frac{\pi n_w d_w^2 k_w \left(T_a - T_{ie}\right)}{4\left(t_{wip} + t_{ip} + t_{wop}\right)} \tag{3.42}$$

$$Q_{vp} = \frac{\pi n_{vp} d_{vp}^2 k_{vp} \left(T_a - T_{ie}\right)}{4\left(t_{wip} + t_{ip} + t_{wop}\right)} \tag{3.43}$$

From Equations (3.22) to (3.43) the total required heater power could be determined.

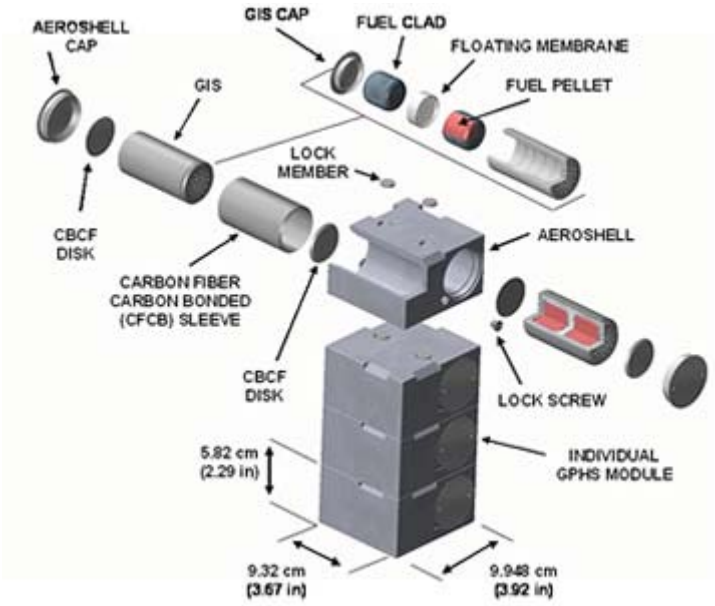

Figure 11.—GPHS block assembly drawing (Ref. 19).

3.4 Power Production

The last area to model in sizing the airship is the amount of power available from the ASRG (Stirling radioisotope powered engine). The Stirling engine converts heat from the isotope blocks to provide electrical power for all of the airship's systems. Each radioisotope block, termed a general-purpose heat source (GPHS), provides 250 W of thermal power at their beginning of life. The blocks are comprised of a number of plutonium-238 pellets, as illustrated in Figure 11. Each block measures 9.95- by 9.32- by 5.82-cm and has a mass of 1.44 kg.

Two blocks are utilized in each ASRG power system as illustrated in Figure 7. The ASRG power systems are enclosed in the upper portion of the payload enclosure as shown in Figure 8 and Figure 10. The output power from each ASRG system (P_{ao}) is dependent on temperature within the ASRG portion of the enclosure as given by Equation (3.44), which is derived from data from Reference 18.

$$P_{ao} = 194.5 - 0.294T_{ia} \tag{3.44}$$

Determining the available power from the ASRG systems is an iterative process between the power produced and the heat loss to the surroundings. The total heat (Q_t) available is the sum of the thermal output of the GPHS blocks within the ASRG systems as given by Equation (3.45). Which is based on the number of ASRG systems (n_a) used considering each ASRG has two GPHS blocks.

$$Q_t = 500n_a \tag{3.45}$$

The total heat generated by the GPHS blocks also must be equivalent to the heat lost and power generated through the following mechanisms, which is represented by Equation (3.46).

- Heat gained from the electronics portion of the payload enclosure
- Heat lost to the atmosphere through the exterior walls of the payload enclosure (Q_{ae})
- Heat gained from the pass-through wires from the Electronics section of the payload enclosure to the ASRG section (Q_{apw})
- The electrical power generated by the ASRGs

$$Q_t = Q_{ae} + P_a - Q_a - Q_{aw} \tag{3.46}$$

The heat loss to the atmosphere through the ASRG portion of the enclosure is calculated in a similar fashion as that for electronics section and is given by Equation (3.47).

$$Q_{ae} = \frac{T_a - T_{ia}}{R_{aiw} + R_{ai} + R_{aow} + R_{aic} + R_{oc}} \tag{3.47}$$

The thermal resistance terms for the different material layers that comprise the ASRG section of the payload enclosure are all similar to those used for the electronics portion, given by Equation (3.29). The corresponding values for the ASRG section to be used with Equations (3.24) to (3.29) are given in Table 9. It should be noted that since the external dimensions of both the ASRG and payload sections of the enclosure are the same, the total thickness variable is calculated from the outer wall inwards by subtracting off the wall and insulation layers.

The interior and exterior convective thermal resistance terms for the ASRG section of the payload enclosure are calculated in the same manner as those for the electronics section, given by Equations (3.32) and (3.33), respectively. The area term for determining the convective resistance terms is given by Equation (3.25) and the variables used are listed in Table 9 for each convective resistance term. The convective coefficients for the ASRG section of the payload enclosure are calculated in a similar manner as those for the electronics section given by Equations (3.34) to (3.35). Since the interior dimensions are different between the two sections the internal height of the ASRG section (h_a) is substituted for the height of the electronics section shown in Equation (3.34).

The heat leak through the pass-through wires from the electronics section to the ASRG section of the payload enclosure is dependent on the number of wires (n_{aw}), their diameter (d_{aw}) and the thermal conductivity of the wire (k_{aw}). Since these are the wires for conducting power they will be larger than the sensor wires used in the electronics section. The heat leak through the wires is given by Equation (3.48).

$$Q_{apw} == \frac{\pi n_{aw} d_{aw}^2 k_{aw} \left(T_i - T_{ia}\right)}{4\left(t_{mlt} + t_{mi} + t_{mut}\right)} \tag{3.48}$$

Since the ASRG section temperature is not known Equations (3.45) to (3.48) are solved iteratively to determine the engine output power.

TABLE 9.—THERMAL RESISTANCE VALUES FOR EACH MATERIAL LAYER IN THE HEAT SOURCE PRESSURE VESSEL

Resistance term (R_t)	Thermal conductivity (k_p)	Layer area (A_{lp})	Perimeter (p_i)	Layer thickness (t_{pwi})	Incremental thickness (d_i)
ASRG section inner wall (R_{aiw})	k_{aiw}	A_{aiw}	p_{aiw}	t_{aiw}	$t_{eiw} + t_{ie} + t_{eow} - t_{aow} - t_{ai}$
ASRG section insulation layer (R_{ai})	k_{ai}	A_{ai}	p_{ai}	t_{ai}	$t_{eiw} + t_{ie} + t_{eow} - t_{aow}$
ASRG section outer wall (R_{aow})	k_{aow}	A_{aow}	p_{aow}	t_{aow}	$t_{eiw} + t_{ie} + t_{eow}$
ASRG Section inner wall convection (R_{aic})	N/A	A_{aiw}	p_{aiw}	t_{aiw}	$t_{eiw} + t_{ie} + t_{eow} - t_{aow} - t_{ai} - t_{aiw}$
ASRG section outer wall convection (R_{oc})	N/A	A_{aow}	p_{aow}	t_{aow}	$t_{eiw} + t_{ie} + t_{eow}$

4.0 Analysis Results

The analysis described in Section 3 was used to evaluate the airship configuration and flight requirements to determine the size, mass and power to operate near the surface of Titan. An initial sizing was performed to provide a baseline design utilizing two ASRG power systems that can fly faster than the wind speed near the surface and provide sufficient heating and power to maintain and operate the payload and electronics. From this design the flight altitude was varied to determine what affect it had on the aircraft sizing.

4.1 Baseline Airship Design

The goal of the baseline airship design was to provide an airship configuration that could operate near the surface of Titan utilizing two ASRG power system modules for providing all the power and heating requirements for the airship. The number of GPHS blocks utilized in the two ASRGs set the available thermal power at 1000 W, which drove all aspects of the design. The baseline airship configuration is shown in Figure 12. This figure represents a proportionally to scale illustration of the airship.

The lifting gas envelope for the airship has an ellipsoidal shape with four control surfaces, fins, symmetrically positioned at the rear of the envelope. Hydrogen is utilized as the lifting gas for the envelope. The payload enclosure is separated into two sections one for the electronics and the other for the ASRG power systems. The payload enclosure is mounted directly to the bottom side of the gas envelope. The electric motor and gearbox are mounted within the payload enclosure to increase their operating temperature and avoid issues with materials and lubrication operating at the ambient Titan conditions. The propeller is connected to the gearbox through a driveshaft. The propeller is located behind the payload enclosure and operates in a pusher configuration.

The payload enclosure specification and the main geometry, characteristics and flight specifications for the airship are listed in Table 10 and Table 11. The mass and power breakdowns are given in Table 12 and Table 13, respectively. The airship was sized so that the available lift and power were equal to or slightly greater than the required lift and power. No additional margin was used in the sizing since power and mass margin was used for sizing of the individual components, as discussed in section 3. For the baseline design the lifting force available for this design point is 344 N, which corresponds to 254.8 kg of mass. The total estimated mass of the airship is 252.7.4 kg, just under the available lift. Similarly the total available power generation capability is 286.8 W, 7.6 W above the required power of 279.2 W.

The drag of the airship is a factor in determining the required airship propulsion power. The drag breakdown for the airship is given in Table 13.

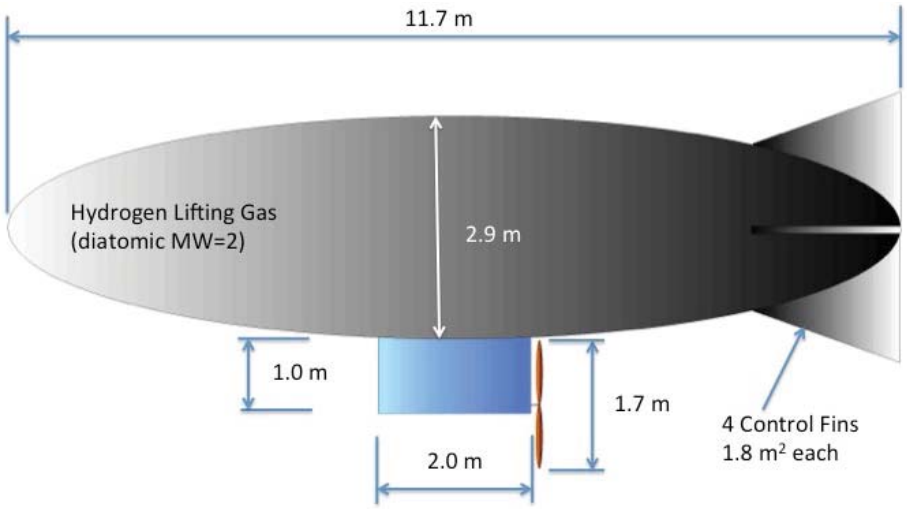

Figure 12.—Baseline airship design dimensions.

TABLE 10.—PAYLOAD ENCLOSURE MATERIAL AND GEOMETRY VARIABLES

Item	Value
Payload enclosure	
ASRG section variables	
Height (h_a)	0.35 m
Inner wall thickness (t_{aiw})	1 mm
Insulation thickness (t_{ai})	1 mm
Outer wall thickness (t_{aow})	1 mm
Upper bulkhead inner wall thickness (t_{uiw})	1 mm
Upper bulkhead insulation thickness (t_{ui})	1 mm
Upper bulkhead outer wall thickness (t_{uow})	1 mm
Inner wall thermal conductivity (k_{aiw})	10 W/mK
Insulation thermal conductivity (k_{ai})	0.017 W/mK
Outer wall thermal conductivity (k_{aow})	10 W/mK
Inner wall density (ρ_{aiw})	1700 kg/m^3
Insulation density (ρ_{ai})	20 kg/m^3
Outer wall density (ρ_{aow})	1700 kg/m^3
Upper bulkhead inner wall density (ρ_{uiw})	1700 kg/m^3
Upper bulkhead insulation density (ρ_{ui})	20 kg/m^3
Upper bulkhead outer wall density (ρ_{uow})	1700 kg/m^3
Structural wall material	Carbon Fiber Composite
Insulation material	Aerogel
Number of wire pass-through (n_{wa})	4
Wire material and thermal conductivity (k_{wa})	Copper: 401 W/mK
Wire diameter (d_{wa})	2.6 mm (10 gauge)
Electronics section variable	
Height (h_e)	0.65 m
Interior length (L_e)	2 m
Interior max width (W_e)	1 m
Inner wall thickness (t_{eiw})	1 mm
Insulation thickness (t_{ei})	11.7 cm
Outer wall thickness (t_{eow})	1 mm
Lower bulkhead inner wall thickness (t_{liw})	1 mm
Lower bulkhead insulation thickness (t_{li})	11.7 cm
Lower bulkhead outer wall thickness (t_{low})	1 mm
Middle bulkhead upper wall thickness (t_{muw})	1 mm
Middle bulkhead insulation thickness (t_{mi})	12 cm
Middle bulkhead lower wall thickness (t_{mlw})	1 mm
Inner wall thermal conductivity (k_{eiw})	10 W/mK
Insulation thermal conductivity (k_{ei})	0.017 W/mK
Outer wall thermal conductivity (k_{eow})	10 W/mK
Middle bulkhead upper wall thermal conductivity (k_{muw})	10 W/mK
Middle bulkhead insulation thermal conductivity (k_{mi})	0.017 W/mK
Middle bulkhead lower wall thermal conductivity (k_{mlw})	10 W/mK
Inner wall density (ρ_{eiw})	1700 kg/m^3
Insulation density (ρ_{ei})	20 kg/m^3
Outer wall density (ρ_{eow})	1700 kg/m^3
Lower bulkhead inner wall density (ρ_{liw})	1700 kg/m^3
lower bulkhead insulation density (ρ_{li})	20 kg/m^3
Lower bulkhead outer wall density (ρ_{low})	1700 kg/m^3
Middle bulkhead inner wall density (ρ_{miw})	1700 kg/m^3
Lower bulkhead insulation density (ρ_{mi})	20 kg/m^3
Lower bulkhead outer wall density (ρ_{mow})	1700 kg/m^3
Structural wall material	carbon fiber composite
Insulation material	Aerogel
Number of wire pass-through (n_w)	30
Wire material and thermal conductivity (k_w)	Copper: 401 W/mK
Wire diameter (d_w)	1 mm (18 gauge)
Number of view ports (n_{vp})	2
View port material and thermal conductivity (k_{vp})	Pyrex Glass: 1.4 W/mK
View port diameter (d_{vp})	10 cm

TABLE 11.—BASELINE AIRSHIP
PHYSICAL CHARACTERISTICS

Item	Value
Airship general specifications	
Airship fineness ratio (length to max diameter)	4
Flight altitude	1 km
Flight velocity (2.25 m/s faster than the estimated average wind speed)	2.38 m/s
Lifting gas	Hydrogen (diatomic)MW=2
Airship envelope length	11.66 m
Airship envelope maximum diameter	2.92 m
Airship envelope volume	51.7 m^3
Total lifting force (mass)	340.7 N (251.9 kg)
Number of control fins	4
Tail fin area (per fin)	1.83 m^2
Envelope material	Metalized Foil 0.25 kg/m^2
Propulsion/Power System	
Propeller diameter	1.69 m
Propeller advance ratio	0.56
Thrust coefficient	0.034
Power coefficient	0.026
Propeller tip Mach number	0.07
Propeller efficiency	0.71
Total driveline efficiency	0.56
Number of ASRG power systems (n_{asrg})	2

TABLE 12.—BASELINE AIRSHIP MASS BREAKDOWN

Item	Mass (kg)
Structure (includes envelope, fins and structural support)	87.0
Electric motor	0.5
Gearbox	0.5
Motor controller	0.1
Motor power conditioning	0.2
Propeller	2.7
ASRG Engine Systems	50
Flight control computer and electronics	3.8
Communications equipment	4.6
Sensors and data acquisition	3.5
Payload/science equipment	25
Payload enclosure (ASRG and electronics sections)	54.2
Lifting gas	20.6
Total mass	**252.7**

TABLE 13.—AIRSHIP DRAG BREAKDOWN

Item	Drag (N)
Electronics and payload enclosure	2.89
Airship lifting gas envelope	5.50
Airship tail	0.92
Total drag	**9.39**

The heat flow from the electronics and ASRG sections of the payload enclosure is illustrated in Figure 13. The values of the parameters, such as the convective heat transfer coefficient, Reynolds number and Nusselt number, used to determine the heat transfer to and from the payload enclosure are given in Table 15.

TABLE 14.—BASELINE AIRSHIP POWER PRODUCTION AND CONSUMPTION

Variable	Value
Power production related variables	
Total thermal power	1000 W
ASRG section internal temperature (T_{ia})	184.3 K
Total ASRG power produced	280.6 W
Power consumption related variables	
Electronics section internal temperature	265 K
ASRG section heat loss through the walls and insulation to exterior	740.5 W
ASRG section pass-through wire heat leak in from electronics section	5.6 W
Electronics section heat loss to exterior	113.8 W
Electronics section pass-through wires heat leak	13.4 W
Electronics section view port heat leak	31.2 W
Electronics section heat loss to ASRG section	15.6 W
Communications, control and payload power	85.0 W
Propulsion system power	71.6 W
Total power required	**280.6 W**

TABLE 15.—CHARACTERISTIC FLOW AND HEAT TRANSFER VALUES FOR THE PAYLOAD ENCLOSURE

Variable	Electronics enclosure section	ASRG enclosure section
Nusselt number	4356 exterior 47.57 interior	4356 exterior 40.64 interior
Reynolds number	3.88×10^{6} exterior	3.88×10^{6} exterior
Prandlt number	0.83 exterior 0.66 interior	0.83 exterior 0.70 interior
Raleigh number	2.93×10^{8} interior	1.68×10^{8} interior
Convective heat transfer coefficient (W/m^2K)	17.5 exterior 1.84 interior	17.5 exterior 2.09 interior

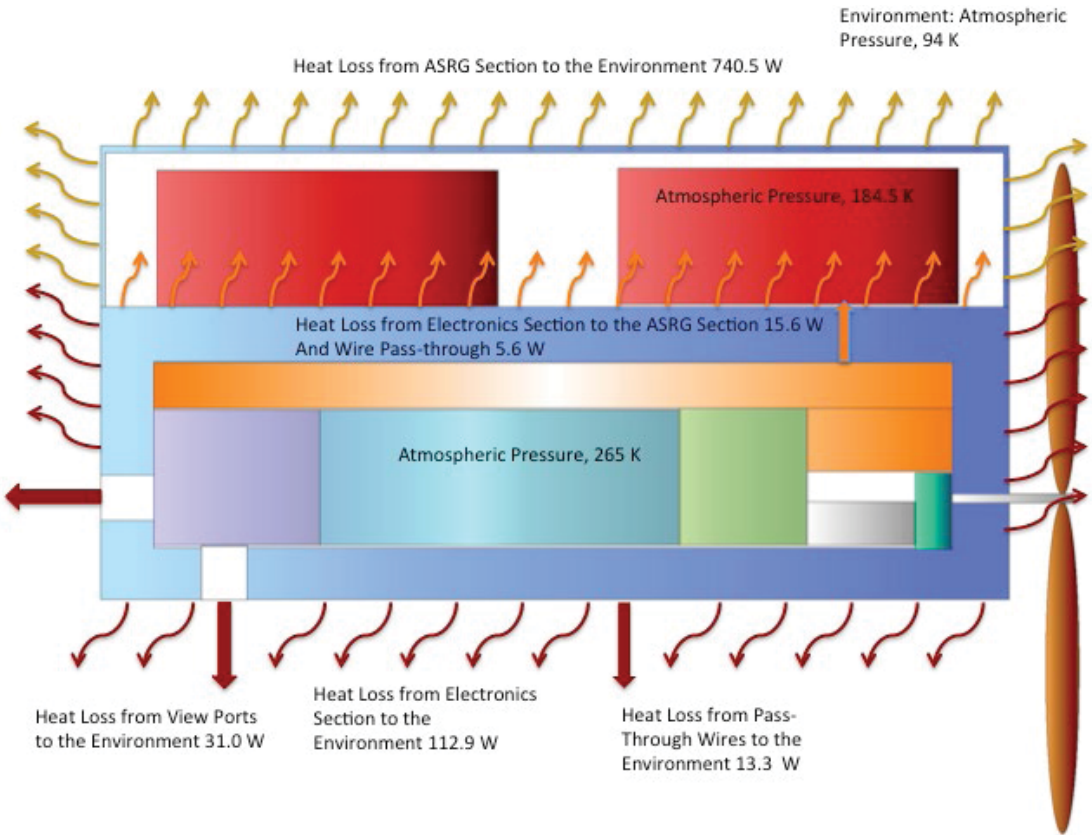

Figure 13.—Heat flow into and out of the payload enclosure.

The results are based on an estimated power level for the science, internal vehicle operations and communications. However the distribution of that total power can be adjusted between those systems as needed to meet the demands of the mission. The only constraint on this is that the power for the communications system was not included in the waste heat utilized to help maintain the internal temperature at the desired level.

For example if additional power is needed for short periods of time for communications or data processing then, based on these results, the airship could move to an altitude that requires less propulsion and heating power. Or the airship could reduce its airspeed to provide additional power for communication or other activities. It is assumed that the power consumed by the propulsion system does not provide any internal heating of the payload enclosure. Therefore reducing the propulsion system power consumption and increasing the communications system output does not affect the internal temperature of the enclosure.

4.2 Variation from the Baseline Design

Changing the input variables of the baseline design can have a significant effect on the airship sizing. The two main parameters that will be affected by changes in the input variables are the gas envelope size and the insulation thickness of the electronics section of the payload enclosure. Changes in envelope size produce changes to the airship lift whereas changes to the insulation thickness produce changes in the power consumption by the heaters. Because the output power of the ASRG systems is mostly fixed the only means to accommodate changes in power demand is to reduce that demand from one of the loads on the airship. For the baseline case these power system loads are shown in Figure 14. The heater power is the only item that can be adjusted without changing the mission or operation of the airship. It can be adjusted by changing the insulation thickness on the electronics section of the payload enclosure.

Adjusting these two items, airship length and insulation thickness, enables variations from the baseline case to be evaluated.

4.2.1 Variation of Electronics Section Operating Temperature

One of the main requirements that drive the airship design is the temperature within the electronics and payload enclosure. For the baseline case this temperature was set at 265 K. To achieve this temperature both waste heat from the electronics and electrically powered heaters were utilized. The temperature difference, between the interior and the surrounding, plays a large role in the power required as well as the size of the enclosure, due to the required insulation thickness. The heating power is dependent on this temperature difference and the subsequent heat leak out to the surroundings from the insulation, wires, view ports and the ASRG section of the payload enclosure. The breakdown of heat loss from the electronics section is broken down in Figure 15.

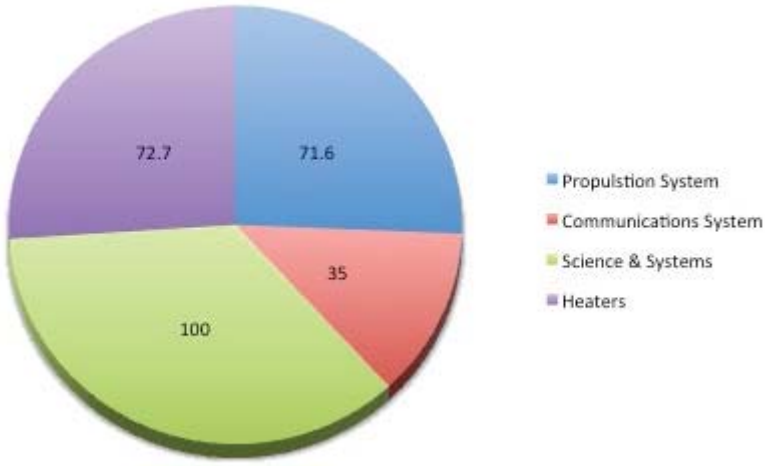

Figure 14.—Power breakdown in Watts for the baseline case operation.

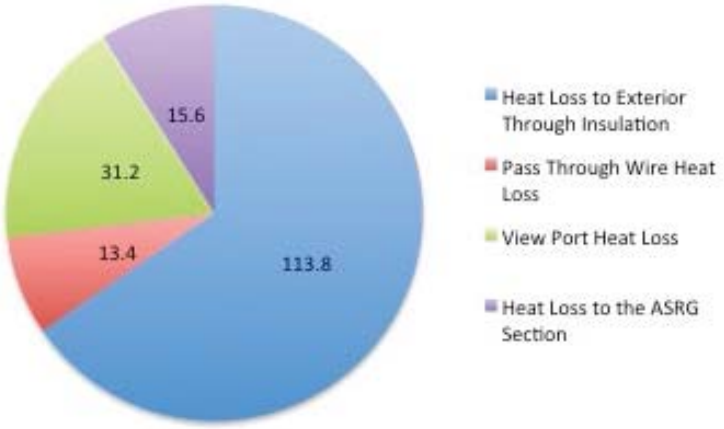

Figure 15.—Baseline case heat loss from the electronics section of the payload enclosure.

The heat loss to the environment is directly related to the amount of insulation within the payload enclosure. For the interior dimensions specified in the baseline case, the amount of insulation determines the exterior dimensions, which in turn affects the mass and drag, the larger the enclosure outside dimensions the greater, its mass and drag.

The waste heat and heater power needed to make up the heat losses shown in Figure 15 are the main power consuming items of the airship operation, as shown in Figure 14. This figure shows the power breakdown for the baseline case. From this figure it can be seen that the heater power consumes approximately 73 W, 26 percent of the total power required. This is in addition to the 100 W of waste heat that is also utilized to make up for the heat loss to the environment.

The ASRG heat sources provide the total amount of available heat. Ultimately all of this heat is released to the environment or converted to electrical power and transmitted through the communications system. The resistance of the heat flow to the environment will set the steady state interior temperature of the payload enclosure. Therefore, to adjust this temperature the resistance to heat flow has to be adjusted up or down. Since, as shown in Figure 15, the greatest mechanism for heat loss is through the insulation, changing the insulation thickness will adjust the internal temperature of the payload enclosure. By changing the insulation thickness the mass and drag of the payload enclosure will also change. This will affect the overall required size of the airship, as shown in Figure 16.

From Figure 16 it can be seen that increasing the internal temperature of the enclosure does increase the airship size but not significantly. The insulation thickness does increase significantly but since it is on the outside of the enclosure there is no reduction in the internal volume. This indicates that operating the electronics section at a higher temperature than that of the baseline case of 265 K would not have a significant effect on the airship or its performance. Changing the operating temperature by 25 K increased the airship length by only 0.8 percent. Therefore, electronics operating temperatures of around 290 K, which are more consistent with conventional spacecraft designs can be considered.

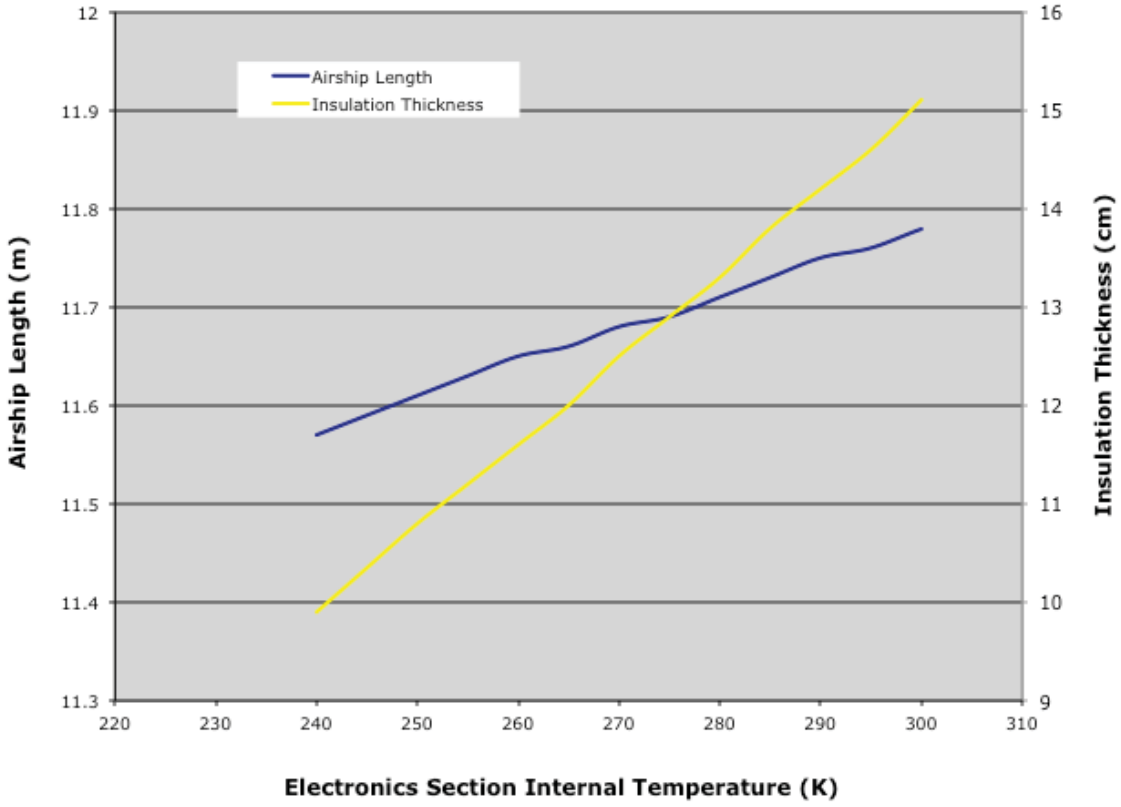

Figure 16.—Required airship length and insulation thickness for a range of electronic section internal temperatures.

4.2.2 Variation in Flight Altitude

The baseline case was sized for operating at an altitude of 1 km. To examine the operation at other altitudes the airship was sized for flight at altitudes above and below the baseline case. The airship length was varied from the baseline length in order to provide sufficient lift at the different altitudes. By changing altitude the environmental conditions, such as the ambient temperature, atmospheric density and wind velocity, changed. The required airship length and corresponding total mass is shown in Figure 17 for an altitude range of 100 m up to 7.64 km, 1 km flight altitude was used in the baseline case. All aspects of the airship, except the dimensions of the gas envelope, remained at the baseline design values. Varying its length changed the volume of the lifting gas envelope. The lifting gas envelope proportions used for the baseline case remained the same.

Figure 17 shows that there is a fairly linear increase in airship length and corresponding mass with increasing flight altitude. This result would be expected since as the altitude increases the atmospheric density decreases fairly linearly at the lower altitudes, as shown in Figure 3. Therefore the lifting force decreases requiring increased lifting gas volume.

As the flight altitude is increased the insulation thickness also needed to increase to maintain the desired temperature within the electronics section of the payload enclosure. This was due to two factors; the increasing wind speed and the decreasing atmospheric temperature with altitude as shown in Figure 3. The higher flight speed and lower atmospheric temperature caused an increase in the convective heat transfer from the outside of the enclosure to the atmosphere. Due to this increased heat transfer the insulation thickness increases significantly with altitude as can be seen in Figure 17.

The maximum altitude achievable by the airship was 7.64 km. Beyond this altitude there was no converged solution to the required airship size for the available power from two ASRG power systems.

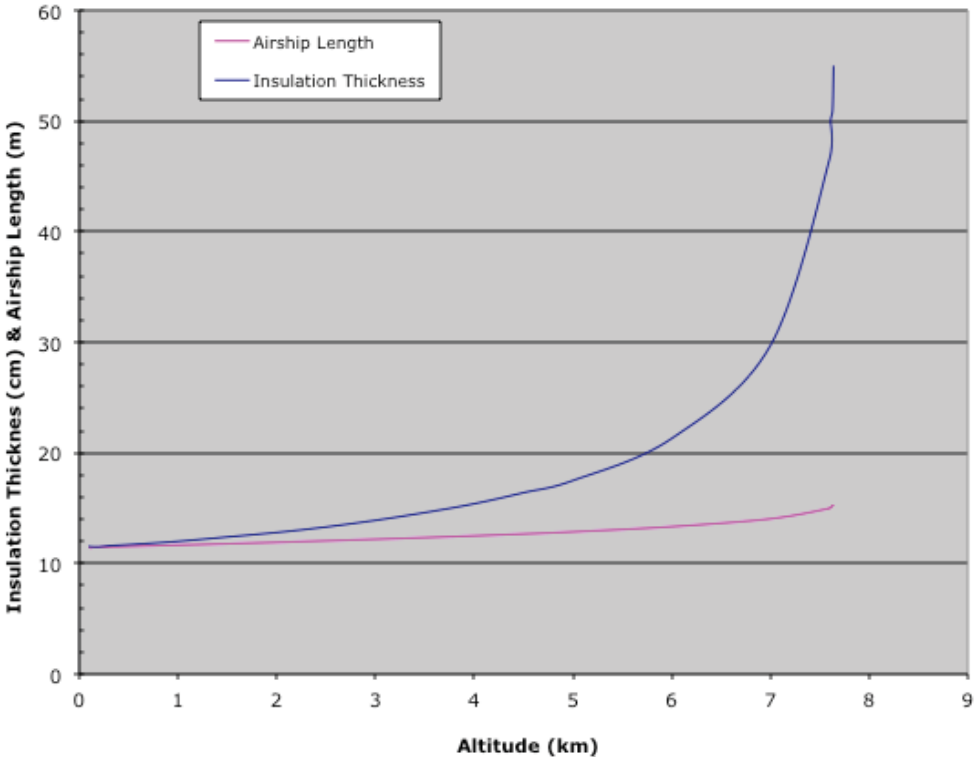

Figure 17.—Required electronics section insulation thickness and airship length for a range of flight altitudes.

Since the insulation thickness and required airship length decrease as altitude decreases, an airship sized for a particular altitude should be able to descent to near the surface. Therefore increasing the airship size and insulation expands the flight envelope of the airship.

This altitude analysis shows that small increases in the airship size can provide large benefits in increasing altitude range. For example an airship 7.2 percent longer (12.5 m versus the baseline airship length of 11.66 m) can provide an increase in maximum altitude from 1 km up to 4 km.

4.2.3 Variation in Payload Mass and Volume

The payload mass for the baseline case was set at 25 kg. Changing this mass will affect the size of the airship and the corresponding insulation thickness of the electronics enclosure. It may not seem obvious that increasing the payload mass should have an effect on the insulation but this is due to a second-order effect of the sizing analysis. By increasing the airship size to accommodate the increase in payload mass, the propulsion power also increases due to the increased drag. Therefore the power consumption has to be decreased in order to accommodate the increase in required propulsion power. To achieve this, the insulation thickness is increased to reduce the required heater power. This change in airship length and insulation thickness for a range of payload masses from 10 to 100 kg is shown in Figure 18.

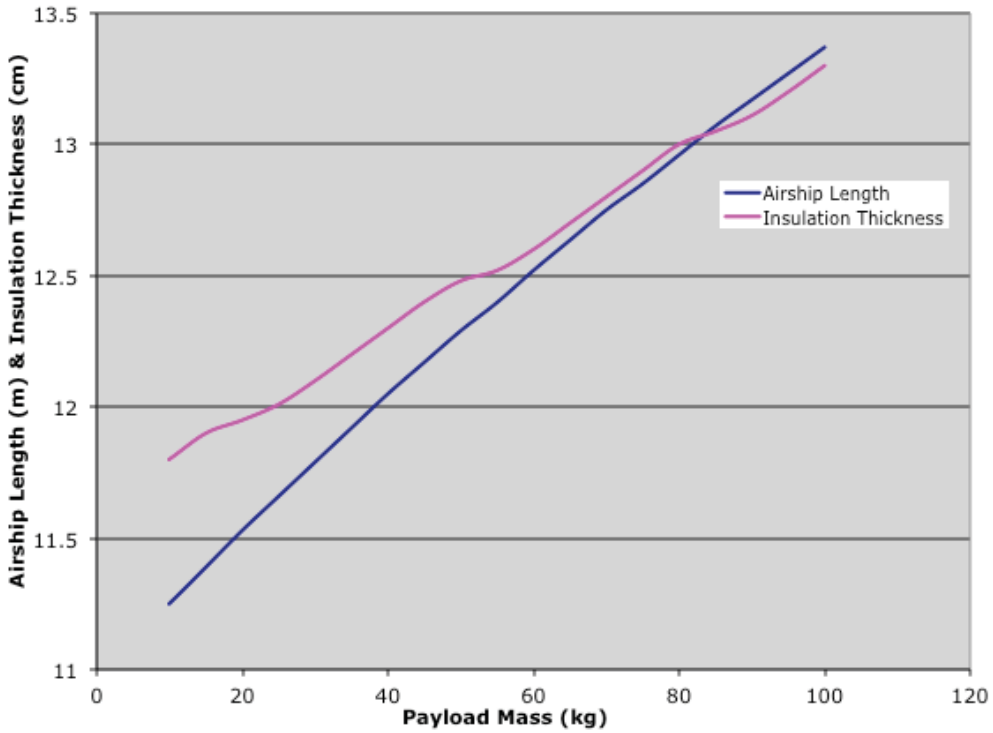

Figure 18.—The change in airship length and insulation thickness with payload mass.

The increase in airship length and insulation thickness is fairly linear with increasing payload mass. There is approximately a 0.6 m increase in airship length for every 25 kg increase in payload mass. The slight step function appearance of the insulation thickness curve is due to the tolerance limits set on the iterative sizing of the airship and insulation.

Either varying the height or length of the payload enclosure or both will change its internal volume. To evaluate how this affects the airship length and required insulation thickness. The payload enclosure length was varied from 2.0 m (the baseline case value) to 4.0 m and the payload height enclosure height was varied from 1.0 m (the baseline case value) to 2.0 m. This changed the internal volume of the payload enclosure from 1.57 to 3.14 m^3. These changes were done separately and the airship length and insulation thickness curves as a function of internal volume are shown in Figure 19 for both cases.

Increasing the internal volume of the payload enclosure caused the airship length and increase as would be expected. The volume change by either an increase in payload enclosure length or height produced a similar rise in airship length through most of the range examined. For a payload enclosure volume greater than 2.8 m^3 there was a slight reduction in airship size by changing the length of the enclosure as compared to changing its height. The insulation thickness also had a benefit of reduced thickness by adjusting the payload enclosure length instead of its height. However this benefit was more pronounced and began at a smaller enclosure volume, approximately 1.9 m^3. These results indicate that if additional internal volume is needed it would be beneficial to increase the payload enclosure length instead of its height. This will minimize the impact of increased payload enclosure volume to the airship sizing.

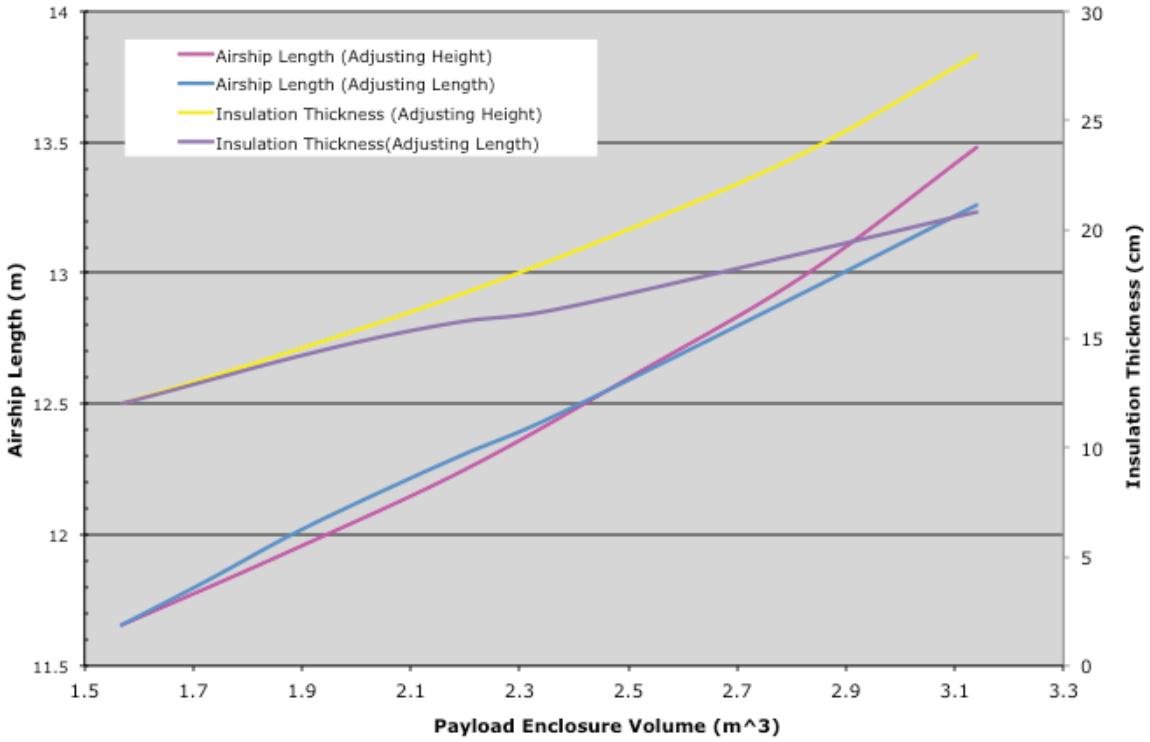

Figure 19.—Change in airship length and insulation thickness for changes in internal volume of the payload enclosure.

5.0 Summary

The goal of this analysis was to determine if an airship, powered by two ASRG power systems, is feasible near the surface of Titan. Based on the airship analysis and design process outlined in Section 3 a baseline airship configuration and size was determined that could meet the mission goals and operate near the Titan surface. This initial analysis indicates that an ASRG powered airship, utilizing hydrogen as the lifting gas, is feasible on Titan. For the baseline design there was sufficient power generated from the two ASRG systems to provide heating and operate the electronics and propulsion system for the airship.

Off design analysis also provided some insight into the benefits that can be gained by altering the vehicle design and operation. It was determined that the airship can be sized to operate up to an altitude of 7.64 km. Beyond this altitude there was no designed solution for an airship with two ASRG power sources. Also since the size of the airship decreased with flight altitude, an airship sized for flight at a specific altitude would be capable of descent to near the surface.

Increasing the interior operating temperature of the electronics section of the payload enclosure did not have a significant effect on the airship size. Therefore if needed, operating the science equipment and electronics at temperatures above the 265 K specified in the baseline case would be feasible.

Other factors, such as changing the payload mass or the internal volume of the payload enclosure, had a much more significant effect on the airship size. Therefore minimizing these would provide benefits to reducing the airship size.

Since this analysis was setup to determine the initial feasibility of the concept there are a number of areas of the design that warrant further more detailed analysis. These would include the following:

- Evaluating the possibility of using the waste heat from the ASRGs to heat the envelope gas to augment the lift produced. This evaluation would have to take into account the affect this would have on the operating temperature of the ASRGs and their corresponding output power. Also

looking at the tradeoff of insulating the gas envelope to increase the gas temperature versus the increased mass and higher operating temperature of the ASRG would provide a net benefit.

- A detailed analysis of the fluid flow over the payload enclosure and airship envelope. The heat transfer from the insulated payload enclosure is a critical factor in the airship sizing. Any change in this value can have a significant effect on the airship design by changing the required heater power. The total power required is also affected by the total vehicle drag. Therefore, this analysis would provide a more accurate determination of the heat transfer from the payload enclosure as well as the drag of the airship itself.
- An optimization of the propeller design for operation within the Titan environment. The propeller was a generic design that was not optimized for Titan. Increasing the propeller efficiency could reduce the propulsion system power requirement.
- A detailed analysis of the internal convection and corresponding heat transfer within the electronics and ASRG sections of the payload enclosure. The heat transfer from the interior gas to the wall of these enclosure sections has a significant effect on the total heat transfer to and from the surroundings and therefore overall vehicle sizing. Providing a higher fidelity analysis of this heat transfer will correspondingly provide a more accurate determination of the airship sizing. This analysis will also provide a means of evaluating methods for reducing the convective heat transfer coefficients. For example by putting natural convection barriers along the internal walls.
- A detailed mechanical design for the airship envelope, gas handling and flight control. If it is desired to have the airship change altitude during flight, a ballast system will have to be incorporated so that the airship can change its buoyancy during operation. This ballast system will require mechanical pumps that would have to operate within the Titan environment. Overall a control scheme for the airship could be developed that would include changing altitude as well as direction. Either utilizing the control fins or directing the propeller thrust or both could perform directional changes.
- The modeling and analysis performed for this report was based on basic physics and thermodynamics. Using this approach the modeling provided a simplified means to evaluate the airship concept. Since the analysis is based on well-established principles the validation of the equations utilized is not necessary. However, there are inherent assumptions incorporated by utilizing this approach that may affect the results. These items, such as incorporating three-dimensional effects into the analysis, can be further evaluated to determine how increased detail and complexity of the analysis would affect the results.

Appendix—Symbols List

A_{ai}	ASRG section insulation surface area
A_{aiw}	ASRG section inner wall surface area
A_{aow}	ASRG section outer wall surface area
A_{ei}	electronics section insulation surface area
A_{eiw}	electronics section inner wall surface area
A_{eow}	electronics section outer wall surface area
A_{la}	middle horizontal surface area
A_{lp}	payload enclosure layer area variable
C_1	viscosity term 1
C_2	viscosity term 2
C_3	viscosity term 3
C_4	viscosity term 4
C_5	viscosity term 5
C_6	viscosity term 6
C_7	thermal conductivity term 1
C_8	thermal conductivity term 2
C_9	thermal conductivity term 3
C_{10}	thermal conductivity term 4
C_{11}	thermal conductivity term 5
D_e	gas envelope drag
D_p	payload enclosure drag
D_t	tail section drag
D_{tot}	total airship drag
L	airship lift
L_e	electronics section interior length
M_{Wa}	atmosphere molecular weight
M_{Wg}	lifting gas molecular weight
Nu_{di}	Payload enclosure internal Nusselt number
Nu_{do}	Payload enclosure external Nusselt number
P_a	atmosphere pressure
P_{ao}	ASRG system output power
P_{ce}	communications equipment power
P_{dt}	drive train system power
P_{fc}	flight control computer power
P_{fs}	flight sensor power
P_h	heating power
P_{pl}	payload power
Pr	atmosphere Prandtl number
P_r	total required power
Pr_i	payload enclosure internal Prandtl number
Q_a	electronics section heat loss to the ASRG section
Q_{ae}	ASRG section atmosphere heat loss
Q_{apw}	ASRG section pass-through wire heat leak
Q_i	electronics section heat loss through the exterior walls
Q_{pt}	electronics section pass through wire heat loss
Q_t	ASRG System GPHS block total heat output
Q_{vp}	view port window heat loss
R	universal gas constant
R_a	atmosphere gas constant

R_{ai} ASRG section insulation thermal resistance
Ra_i payload enclosure internal Rayleigh number
R_{aic} ASRG section internal convection thermal resistance
R_{aiw} ASRG section inner wall thermal resistance
R_{aow} electronics section outer wall thermal resistance
Re_{do} payload enclosure external Reynolds number
R_{ei} electronics section insulation thermal resistance
R_{eic} electronics section internal convection thermal resistance
R_{eiw} electronics section inner wall thermal resistance
R_{eow} electronics section outer wall thermal resistance
Re_p payload enclosure external Reynolds number
R_{mi} middle horizontal insulation thermal resistance
R_{mlw} middle horizontal upper wall thermal resistance
R_{muw} middle horizontal lower wall thermal resistance
R_{oc} external convection thermal resistance
R_t payload enclosure thermal resistance variable
T_a Venus atmospheric temperature
T_g lifting gas temperature
T_{ia} ASRG section internal temperature
T_{ie} electronics section internal temperature
T_{if} payload enclosure internal wall film temperature
U airship velocity
V_a airship envelope volume
W_e electronics section interior width
W_{tot} airship total weight
Z altitude above the surface
a atmosphere speed of sound
c_{de} airship gas envelope drag coefficient
c_{dp} payload enclosure drag coefficient
c_i parameter equation term
c_{pa} atmosphere specific heat
d airship envelope maximum diameter
d_{aw} ASRG section pass through wire diameter
d_i payload enclosure incremental layer thickness variable
d_{vp} view port diameter
d_w pass through wire diameter
f airship envelope fineness ratio
g Titan gravitational acceleration
h_a ASRG section height
h_{ai} ASRG section internal convection coefficient
h_e electronics section height
h_{ei} electronics section internal convection coefficient
h_i payload enclosure section height variable
h_o payload enclosure external convection coefficient
k_a atmosphere thermal conductivity
k_{ai} ASRG section insulation thermal conductivity
k_{aiw} ASRG section inner wall thermal conductivity
k_{aow} ASRG section outer wall thermal conductivity
k_{aw} ASRG section pass through wire thermal conductivity
k_{ei} electronics section insulation thermal conductivity
k_{eiw} electronics section inner wall thermal conductivity

k_{eow} electronics section outer wall thermal conductivity
k_{mi} middle horizontal insulation thermal conductivity
k_{mlw} middle horizontal upper wall thermal conductivity
k_{muw} middle horizontal lower wall thermal conductivity
k_p payload enclosure thermal conductivity variable
k_{vp} view port material thermal conductivity
k_w pass through wire thermal conductivity
l airship envelope length
m_{ai} ASRG Section Insulation Mass
m_{aiw} ASRG Section Inner Wall Mass
m_{aow} ASRG Section Outer Wall Mass
m_{asrg} ASRG Unit System Mass
m_{ce} communication equipment mass
m_{dt} drive train total mass
m_{ei} electronics section insulation mass
m_{eiw} electronics section inner wall mass
m_{eow} electronics section outer wall mass
m_{fc} flight control computer mass
m_{fi} fixed item mass
m_{fs} flight control sensor mass
m_{hw} payload enclosure horizontal wall mass
m_{hwi} payload enclosure horizontal wall mass variable
m_{lg} lifting gas mass
m_{li} lower horizontal insulation mass
m_{liw} lower horizontal inner wall mass
m_{low} lower horizontal outer wall mass
m_{mi} middle horizontal insulation mass
m_{mlw} middle horizontal upper wall mass
m_{muw} middle horizontal lower wall mass
m_{pe} payload enclosure mass
m_{pl} payload mass
m_{pw} payload enclosure elliptical wall mass
m_{pwi} payload enclosure layer mass variable
m_s airship structure mass
m_{tot} total airship mass
m_{ui} upper horizontal insulation mass
m_{uiw} upper horizontal inner wall mass
m_{uow} upper horizontal outer wall mass
n_a number of ASRG systems
n_{aw} number of ASRG section wire pass-throughs
n_{vp} number of view ports
n_w number of pass-through wires
p_{ai} ASRG section insulation parameter
p_{aiw} ASRG section inner wall parameter
p_{aow} ASRG section outer wall parameter
p_{ei} electronics section insulation parameter
p_{eiw} electronics section inner wall parameter
p_{eow} electronics section outer wall parameter
p_i payload enclosure layer parameter variable
t_{ai} ASRG section insulation thickness
t_{aiw} ASRG section inner wall thickness

t_{aow} ASRG section outer wall thickness
t_{ei} electronics section insulation thickness
t_{eiw} electronics section inner wall thickness
t_{eow} electronics section outer wall thickness
t_{hwi} payload enclosure horizontal wall thickness variable
t_{li} lower horizontal insulation thickness
t_{liw} lower horizontal inner wall thickness
t_{low} lower horizontal outer wall thickness
t_{mi} middle horizontal insulation thickness
t_{mlw} middle horizontal lower wall thickness
t_{muw} middle horizontal upper wall thickness
t_{pwi} payload enclosure layer thickness variable
t_{ui} upper horizontal insulation thickness
t_{uiw} upper horizontal inner wall thickness
t_{uow} upper horizontal outer wall thickness
v_a atmosphere wind velocity
ΔT_{wi} payload enclosure inner wall and internal gas temperature difference
α_a atmosphere thermal diffusivity
γ_a atmosphere ratio of specific heats
η_{dt} propulsion system efficiency
μ_a atmosphere dynamic viscosity
ν_a atmosphere kinematic viscosity
ρ_a atmosphere density
ρ_{ai} ASRG section insulation material density
ρ_{aiw} ASRG section inner wall material density
ρ_{aow} ASRG section outer wall material density
ρ_{ei} electronics section insulation material density
ρ_{eiw} electronics section inner wall material density
ρ_{eow} electronics section outer wall material density
ρ_{hwi} payload enclosure horizontal wall density variable
ρ_{li} lower horizontal insulation density
ρ_{liw} lower horizontal inner wall density
ρ_{low} lower horizontal outer wall density
ρ_{mi} middle horizontal insulation density
ρ_{mlw} middle horizontal upper wall density
ρ_{muw} middle horizontal lower wall density
ρ_{pwi} payload enclosure layer material density variable
ρ_{ui} upper horizontal insulation density
ρ_{uiw} upper horizontal inner wall density
ρ_{uow} upper horizontal outer wall density

References

1. Cassini Solstice Mission, Jet Propulsion Laboratory web site, Saturn.jpl.nasa.gov, October 2013.
2. Colozza, A., "Airships for Planetary Exploration," NASA/CR—2004-213345, November 2004.
3. Cassini-Huygens Saturn Arrival Press Kit, NASA, June 2004.
4. Flasar, F.M., et al., "Titan's Atmospheric Temperatures, Winds, and Composition," Science, Vol. 308, pp. 975-978, May 13, 2005.
5. Brown, R.H., Lebreton, J.P. and Waite, J.H. editors, Titan from Cassini-Huygens, Springer Science-Business Media, 2009.
6. Solar System Exploration: Titan (moon), NASA, solarsystem.nasa.gov, March 2013.
7. Bezard, B., Yelle, R.V. and Nixon, C.A., "The Composition of Titan's Atmosphere," Chapter 6, Titan: Surface, Atmosphere and Magnetosphere, Cambridge University Press, 2013.
8. Bird, M.K. et al., "The Vertical Profile of Winds on Titan," Nature, Vol. 438, pp. 800-802, December 8, 2005.
9. Lemmon, E.W., and Jacobsen, R.T., "Viscosity and Thermal Conductivity Equations for Nitrogen, Oxygen, Argon and Air," International Journal of Thermophysics, Vol. 25, No. 1, pp. 21-69, January 2004.
10. Khoury, G.A. and Gillett, J.D., eds., Airship Technology, Cambridge Aerospace Series 10, Cambridge University Press, 1999.
11. Colozza, A.J., "Radioisotope Stirling Engine Powered Airship for Low Altitude Operation on Venus," NASA/CR—2012-217665, August 2012.
12. Colozza, A.J., "Initial Feasibility Assessment of a High Altitude Long Endurance Airship," NASA/CR—2003-212724, December 2003.
13. Colozza, A.J., "Comparison of Mars Aircraft Propulsion Systems," NASA/CR—2003-212350, May 2003.
14. Advanced Stirling Radioisotope Generator, ASRG Fact Sheet, National Aeronautics and Space Administration, www.nasa.gov, February 2010.
15. Cataldo, R.L., Tatro, C.A., Colozza, A.J., Wang, X.Y., and Rusick, J.J. "Concept of Operations for the Advanced Stirling Radioisotope Generator," NETS 2012: Nuclear and Emerging Technologies for Space, Paper 3074, March 21-23, 2012.
16. Zukauskas, A. and Karni, J., High-Performance Single Phase Heat Exchangers, Taylor and Francis, 2001.
17. Incropera, F.P., and DeWitt, D.P., Fundamentals of Heat and Mass Transfer, Third Edition, John Wiley & Sons Publisher, 1990.
18. Lockheed Martin Spacer Systems, "Engineering Unit Advanced Stirling Radioisotope Generator Expanded Missions Capability Study," Contract No. DE-AC07-00SF22191, August 2008.
19. "Space and Defense Power Systems," U.S. Department of Energy, www.ne.doe.gov, October 2011.